Zonally Asymmetric Temperature Trends near the Northern Middle and High Latitude Stratopause during Winter

Journal:	*Journal of Meteorological Research (JMR)*
Manuscript ID	ACTA-E-2023-0015.R2
Manuscript Type:	Original Article
Date Submitted by the Author:	19-Apr-2023
Complete List of Authors:	Wang, Tao; Lanzhou University, colledge of atmospheric science Tian, Wenshou; Lanzhou University, colledge of atmospheric science Zhang, Ruhua; Fudan University, Department of Atmospheric and Oceanic Sciences and Institute of Atmospheric Sciences Luo, Jiali; Lanzhou University, College of Atmospheric Sciences Feng, Wuhu; University of Leeds, School of Chemistry
Keywords:	Stratospheric temperature trend, zonally asymmetric temperature pattern, quasi-stationary planetary wavenumber 1
Speciality:	Stratospheric climate changes, Atmospheric dynamics

Zonally Asymmetric Temperature Trends near the Northern Middle and High Latitude Stratopause during Winter

Tao WANG[1], Wenshou TIAN[1*], Ruhua ZHANG[2], Jiali LUO[1], and Wuhu FENG[3]

1 *College of Atmospheric Sciences, Lanzhou University, Lanzhou* 730000, *China*

2 *Department of Atmospheric and Oceanic Sciences and Institute of Atmospheric Sciences, Fudan University, Shanghai* 200438, *China*

3 *National Centre for Atmospheric Science (NCAS), School of Earth and Environment, University of Leeds, Leeds LS2 9JT, UK*

Received 29 January 2023; revised 21 March 2023; accepted 21 April 2023

Supported partly by the National Natural Science Foundation of China (42130601 and 42142038).

*Corresponding author: wstian@lzu.edu.cn

Abstract

The temperature trend near the stratopause is rarely evaluated owing to the limited long-term observations of global temperature. In this study, the spatial patterns of the temperature trends near the stratopause are investigated using satellite and reanalysis datasets. Our analysis reveals a zonally asymmetric temperature trend pattern near the northern mid-to-high latitude stratopause during January, and this pattern underwent an evident transition around the 2000s. From 1980 to 2003, there was a cooling trend in the western hemisphere and a warming trend in the eastern hemisphere. In contrast, a reversed zonally asymmetric temperature trend pattern existed in the east-west direction from 2003 to 2020. Although the warming trends are statistically insignificant, they contrasted with the overall cooling trend in the upper stratosphere due to ozone depletion and an increase in well-mixed greenhouse gases in recent decades. The zonally asymmetric temperature trends were induced by the transition in the intensity of quasi-stationary planetary wavenumber 1 (wave 1) near the stratopause. The increasing (decreasing) trend of the intensity of wave 1 enhanced (reduced) its meridional temperature advection near the stratopause before (after) the 2000s, consequently, a zonally asymmetric temperature trend pattern exists in the east-west direction near the stratopause. The transition in the intensity of the stratospheric wave 1 around the 2000s is most likely caused by the transition in the intensity of wave 1 activity in the troposphere.

Key words: Stratospheric temperature trend, zonally asymmetric temperature pattern, quasi-stationary planetary wavenumber 1

Citation: Wang, T., W. S. Tian, R. H. Zhang, et al., 2023: Zonally asymmetric temperature trends near the northern middle and high latitude stratopause during winter. *J. Meteor. Res.*, **37**(x), XXX－XXX, doi: 10.1007/s13351-023-3015-8.

1. Introduction

The stratospheric temperature is a crucial climate marker that is affected by both thermal-dynamic and chemical processes. In response to ozone depletion and increasing well-mixed greenhouse gases (GHGs), the stratospheric temperature has experienced a significant cooling trend over the past several decades, which has been noted by a wide variety of observations and reproduced by multiple climate models (e.g., Golitsyn et al., 1996; Ramaswamy et al., 2001; Wang et al., 2012; Thompson et al., 2009, 2012; Randel et al., 2009, 2017; Rao et al., 2015; Garcia et al., 2019; Remsberg, 2019; Steiner et al., 2020). Notably, recently updated and extended satellite data has provided relatively reliable zonal mean temperature observations throughout the stratosphere and revealed that the zonal mean temperature trends decreased with altitude from the lower stratosphere to the upper stratosphere from 1979 to 2015 (McLandress et al., 2015; Randel et al., 2016; Zou and Qian, 2016). However, the long-term trends in stratospheric temperature still have uncertainties in both their magnitudes and spatial variations (e.g., Shine et al., 2003; Fu et al., 2010; Seidel et al., 2011; Funatsu et al., 2016; Maycock et al., 2018). These uncertainties are partly due to discrepancies in different observations (e.g., Zou et al., 2009; Thompson et al., 2012; Keckhut et al., 2019; Seidel et al., 2016) and are partly relate to the challenges involved in clarifying the factors that contribute to stratospheric temperature trends (e.g., Hu and Fu, 2009; Hu et al., 2009; Ivy et al., 2016; Xia et al., 2020; Zhou et al., 2022).

Various factors may influence temperature trends in the stratosphere. Although well-mixed GHGs are still increasing, a weak recovery signal has appeared in

stratospheric ozone in the last two decades (e.g., Hu et al., 2015; Chipperfield et al., 2017). Consequently, future trends in stratospheric temperatures (Arblaster et al., 2014; WMO, 2018) will mainly result from the opposing effects of increasing CO_2 (colder stratosphere) and increasing ozone (the warmer stratosphere). Moreover, the increasing stratospheric water vapor and volcanic aerosols have potentially impacted the temperature trends in the tropical lower stratosphere in recent decades (e.g., Maycock et al., 2014). Apart from the radiative contributions of chemical constituents, dynamic processes also have a large impact on stratospheric temperature trends, particularly at middle and high latitudes. It is known that temperatures in the stratosphere at middle and high latitudes are dominated by both the radiative balance and dynamic heating originating from tropospheric wave forcing (Andrews et al., 1987; Haynes, 2005; He et al., 2022). Given that GHGs trends are monotonically increasing, the temperature trends in the stratosphere at middle and high latitudes are strongly modulated by changes in planetary wave forcing in the stratosphere (Hu and Tung, 2002; Fu et al., 2019). As a result, the large interannual and decadal variations in dynamical forcing may lead to large uncertainties in stratospheric temperature trends (e.g., Matsuno, 1971; Yamashita et al., 2010; Long et al., 2017).

On the other hand, previous studies have mainly focused on trends in global or zonal mean temperatures in the stratosphere, but the longitudinal variations in the temperature trend in the stratosphere have rarely been evaluated. In particular, the spatial variations in the temperature trend near the stratopause are still poorly understood due to the shortage of long-term global observations there. It is well known

that the polar night jet is persistent in the Northern Hemisphere (NH) winter, indicating strong baroclinicity there (France and Harvey, 2013; Harvey et al., 2002). Harvey and Hitchman (1996) noted that the maximum longitudinal differences between the Aleutian High and the polar vortex were located near the stratopause. In addition, previous studies have reported the shift in the tropospheric and stratospheric climate around the 2000s (e.g., Chen and Tung, 2014; Hu et al., 2019). However, whether the climate shift occurs near the stratopause is still unclear. Therefore, it is of interest to investigate the changes in the temperature near the stratopause in recent decades.

In this study, we employ the Modern-Era Retrospective Analysis for Research and Applications, version 2 (MERRA-2) reanalysis datasets from 1980 to 2020 and the TIMED/SABER satellite temperature data from 2003 to 2020 to investigate spatial variations in the temperature trend near the stratopause during the northern winter as well as the possible factors responsible for the temperature trends near the stratopause. The organization of our paper is as follows. Section 2 describes the data and method we used. In Section 3, we exhibit and compare the temperature trends near the stratopause during the northern winter derived from TIMED/SABER observations and the MERRA-2 reanalysis dataset. In Section 4, we investigate possible factors responsible for the temperature trends. The conclusions and discussions are summarized in Section 5.

2. Data and Methods

2.1 Data

SABER is an infrared limb sounder launched on the TIMED satellite, which provides reliable global temperature data above the troposphere. Its latitudinal coverage ranges from a north-looking mode (53°S–83°N) to a south-looking mode (53°N–83°S) approximately every 60 days. The SABER temperature profiles have been retrieved from infrared emissions of CO_2 from approximately 16 km to 105 km altitude with an effective vertical resolution of 2 km. TIMED/SABER temperature has been evaluated by Remsberg et al. (2003, 2008). In this study, we use the TIMED/SABER (version 2.0) temperature dataset from 2003 to 2020 and bin the data into 2° × 4° (longitude by latitude) monthly mean maps.

MERRA-2 is produced by the National Aeronautics and Space Administration (NASA) Global Modeling and Assimilation Office (GMAO). The temperature data from the Microwave Limb Sounder (MLS) are assimilated in MERRA-2 above 5 hPa, providing more accurate temperature data for the upper stratosphere than MERRA (Gelaro et al. (2017). The zonal mean temperature comparisons between observations and reanalysis datasets, including MERRA-2, were investigated by Long et al. (2017). The MERRA-2 instM_3d_asm_Np monthly mean datasets (Version 5.12.4) are used during the period from 1980 to 2020, with a horizontal resolution of 0.5° × 0.625° (latitude × longitude) and 42 vertical levels up to a height of 0.1 hPa.

2.2 Method

In this study, the Eliassen-Palm (EP) flux (Andrews et al., 1987) and the Plumb flux (Plumb, 1985) are applied to measure the strength and propagation of wave activities in two dimensions and three dimensions, respectively. The meridional ($F^{(\varphi)}$)

and vertical ($F^{(z)}$) components of the EP flux and its divergence ($\nabla \cdot \boldsymbol{F}$) are defined as follows:

$$F^{(\varphi)} = \rho_0 a\cos\varphi\left(\overline{u}_z \frac{\overline{v'\theta'}}{\overline{\theta}_z} - \overline{u'v'}\right) \quad (1)$$

$$F^{(z)} = \left(f - \frac{(\overline{u}\cos\varphi)_\varphi}{a\cos\varphi}\right)\frac{\overline{v'\theta'}}{\overline{\theta}_z} - \overline{u'w'} \quad (2)$$

$$\nabla \cdot \boldsymbol{F} = \frac{\partial F^{(\varphi)}}{\partial \varphi} + \frac{\partial F^{(z)}}{\partial z} \quad (3)$$

where φ is latitude, z is height, ρ is air density, a is the Earth's radius, f is the Coriolis parameter, θ is potential temperature, u is zonal wind, v is meridional wind, and w is vertical wind. The overbars and primes denote the zonal mean and the departure from the zonal mean, respectively. The subscript 0 is for the background variables. The subscript z is for the partial derivative for the variables in the vertical direction.

The longitude ($F^{(\lambda)}$), latitude ($F^{(\varphi)}$), and vertical ($F^{(z)}$) components of the Plumb flux and its divergence ($\nabla \cdot \boldsymbol{F}$) are defined as follows:

$$F^{(\lambda)} = \rho_0 \cos\varphi \; \left(\frac{1}{2a^2\cos^2\varphi}\left[\left(\frac{\partial \psi'}{\partial \lambda}\right)^2 - \psi' \frac{\partial^2 \psi'}{\partial \lambda^2}\right]\right) \quad (4)$$

$$F^{(\varphi)} = \rho_0 \cos\varphi \; \left(\frac{1}{2a^2\cos^2\varphi}\left[\frac{\partial \psi'}{\partial \lambda}\frac{\partial \psi'}{\partial \varphi} - \psi' \frac{\partial^2 \psi'}{\partial \lambda \partial \varphi}\right]\right) \quad (5)$$

$$F^{(z)} = \rho_0 \cos\varphi \; \left(\frac{2\Omega^2 \sin^2\varphi}{N^2 a\cos\varphi}\left[\frac{\partial \psi'}{\partial \lambda}\frac{\partial \psi'}{\partial z} - \psi' \frac{\partial^2 \psi'}{\partial \lambda \partial z}\right]\right) \quad (6)$$

$$\nabla \cdot \boldsymbol{F} = \frac{\partial F^{(\lambda)}}{\partial \lambda} + \frac{\partial F^{(\varphi)}}{\partial \varphi} + \frac{\partial F^{(z)}}{\partial z} \quad (7)$$

where λ is longitude, Ω is the Earth's angular velocity, N is the Brunt–Väisälä frequency, $\psi = \Phi/2\Omega\sin\varphi$, and Φ is potential height.

3. Temperature Trends Near the Stratopause during the

Northern Winter

Figs. 1a and 1c present the spatial patterns of the 3 hPa temperature trends over the NH during January from 1980-2003 and from 2003-2020 derived from MERRA-2 reanalysis data, respectively. A noticeable feature is that there is a zonally asymmetric pattern in temperature trends at mid-high latitudes shown in Fig. 1a, with a cooling trend in the western hemisphere and a warming trend in the eastern hemisphere. In contrast, a reversal temperature trend in the east-west direction can be noted in Fig. 1c, with a warming (cooling) trend in the western (eastern) hemisphere. Note that the results here are not sensitive to slight changes in the starting/ending year of the time series. Thompson et al. (2012) indicated that due to ozone depletion and increasing well-mixed GHGs in recent decades, the stratospheric cooling in the upper stratosphere is more robust than that in the lower-middle stratosphere. Hence, although these warming trends in Figs. 1a and 1c are statistically insignificant at the 95% confidence level, they contrast with the overall cooling trend in the upper stratosphere. To understand the unusual warming near the stratopause, we separate the temperature into two components, i.e., zonal mean and deviations from the zonal mean (hereafter zonal temperature deviations). The zonal mean temperature denotes the background field, which is dominated by chemical and radiative balances. The temperature deviations denote the disturbed field, which is largely controlled by adiabatic/diabatic thermodynamic processes.

Figs. 1b and 1d show the spatial patterns of trends in zonal temperature deviations at 3 hPa over the NH during January from 1998 to 2003 and from 2003 to 2020 derived from MERRA-2 reanalysis data, respectively. The trends in zonal temperature deviations also present zonally asymmetric patterns at mid-high latitudes, with a statistically significant cooling (warming) trend in the western (eastern) hemisphere in Fig. 1b, and a reversal temperature trend in the east-west direction in Fig. 1d. The warming (cooling) trends in the zonal temperature deviations are stronger (weaker) compared to those in the original temperature. The green counters superimposed on Figs. 1b and 1d are the climatology of the zonal temperature deviations, which are likewise zonally asymmetric at mid-high latitudes, with negative (positive) anomalies in the western (eastern) hemisphere. The climatology of the zonal temperature deviations is generally in phase (out of phase) with the trends of the zonal temperature deviations in Fig. 1b (1d), suggesting that the zonal asymmetry of temperature variations was strengthened (weakened) before (after) the 2000s, and there was a transition in the zonally asymmetric temperature trend pattern around the 2000s.

The latitudinal variations in the 3 hPa zonal mean temperature trends over the NH during January from 1980 to 2003 and from 2003 to 2020 derived from MERRA-2 reanalysis data are shown in Fig. 1g, respectively. The morphology of zonal mean temperature trend before the 2000s is similar to that after the 2000s. The zonal mean temperature trend is close to zero at lower latitudes but decreases with increasing latitudes at mid-high latitudes. Overall, the zonal mean temperature trend before/after the 2000s is cooling in the NH, which is consistent with the increase in well-mixed GHGs in recent decades. The results shown in Fig. 1 as derived from MERRA-2 reanalysis data suggest that the zonal asymmetry of the temperature trends near the stratopause is the product of changes in disturbed fields.

To further verify the trends exhibited in Fig. 1 derived from MERRA-2 reanalysis data, TIMED/SABER satellite temperature observations (from 2003-2020) are analyzed. Figs. e, f, and g (blue line) are the same as Figs. c, d, and g (red line), respectively, but the data is derived from TIMED/SABER observations. It is seen that the zonally asymmetric temperature trend pattern is also apparent in TIMED/SABER observations, and the corresponding results derived from MERRA-2 reanalysis data agree well with those derived from TIMED/SABER observations in both morphology and magnitude. Since the temperature trends near the stratopause in MERRA-2 reanalysis data are in good agreement with those from the TIMED/SABER temperature observations, the MERRA-2 dataset is utilized to investigate the possible factors responsible for the zonally asymmetric variations in the temperature. Note that the spatial pattern of 3 hPa temperature shows an almost uniform cooling trend over the NH during January from 1980 to 2020 derived from MERRA-2 reanalysis data (not shown).

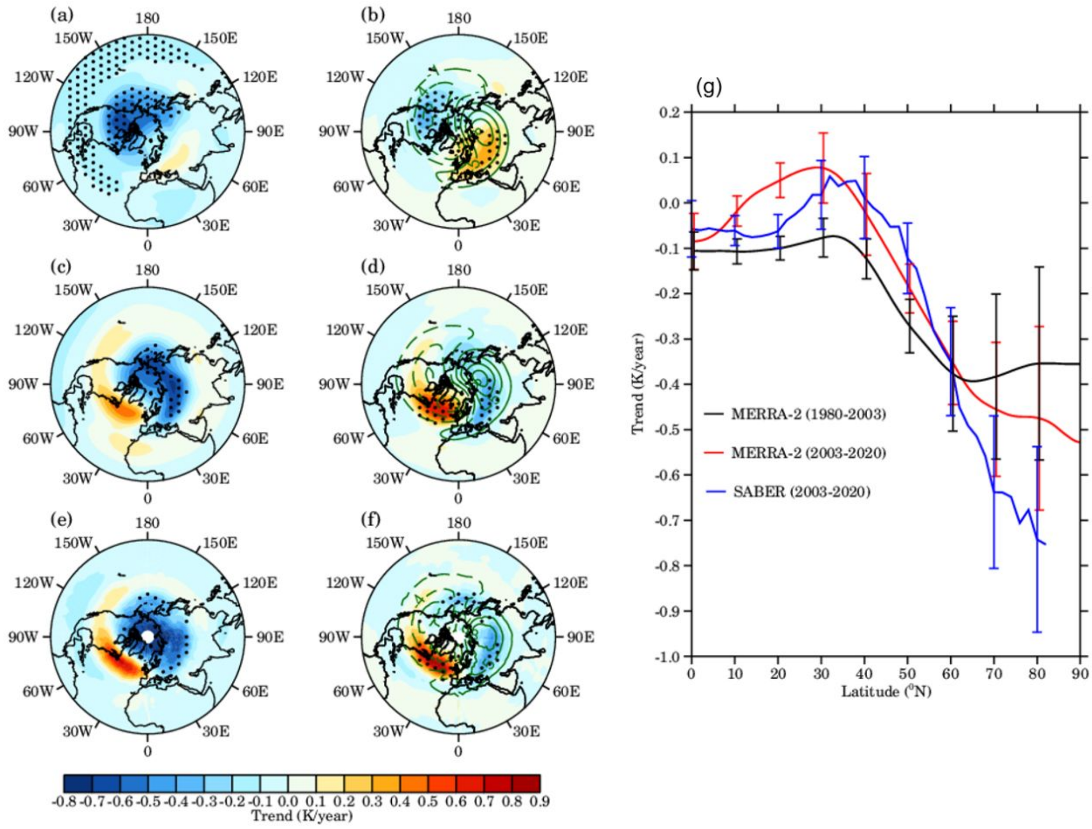

Fig. 1. Spatial pattern of trends in (a) temperature and (b) zonal temperature deviations over the NH at 3 hPa during January from 1980 to 2003 derived from MERRA-2 reanalysis data. (c) and (d) are the same as (a) and (b), respectively, but the time period is from 2003 to 2020. (e) and (f) are the same as (c) and (d), respectively, but the data is derived from TIMED/SABER observations. The values over the stippled areas are statistically significant at the 95% confidence level according to Student's t test. The green contour lines denote the climatology of the zonal temperature deviations (the contour interval is 3 K, solid and dashed lines indicate positive and negative values, respectively). (g) Latitude variations in the zonal mean temperature trends over the NH at 3 hPa during January from 1980 to 2003 derived from MERRA-2 reanalysis dataset (black line), from 2003 to 2020 derived from MERRA-2 reanalysis dataset (red line), and from 2003 to 2020 derived from TIMED/SABER observations (blue line). Error

bars show the 2σ statistical uncertainty.

Fig. 2 presents the time series of the zonal temperature deviations averaged over the climatological high-temperature lobe (hereafter East) (50°N-70°N, 30°E-180°E) (solid lines) and the climatological low-temperature lobe (hereafter West) (50°N-70°N, 0-150°W) (dashed lines) at 3 hPa during January from 1980 to 2020 derived from MERRA-2 reanalysis data (black lines) and from 2003 to 2020 derived from TIME/SABER observations (blue lines), respectively. The straight lines represent the linear fits of the zonal temperature deviations before and after 2003, respectively. The time series of the zonal temperature deviations derived from MERRA-2 agree well with those derived from the TIMED/SABER observations in both magnitudes and variations. The East underwent a statistically significant increasing trend (0.1 K/year) from 1980 to 2003 and a statistically significant decreasing trend (-0.17 K/year) from 2003 to 2020. The West has similar magnitudes but opposite signs in both interannual variations and long-term trends compared to the East, indicating a close negative correlation in the zonal temperature deviations between the two lobes. The correlation coefficients between the East and West are -0.89 (-0.90) derived from the MERRA-2 reanalysis data (TIMED/SABER observations). Note that the results here are not sensitive to slight changes in the latitude/longitude bounds used for averaging the data.

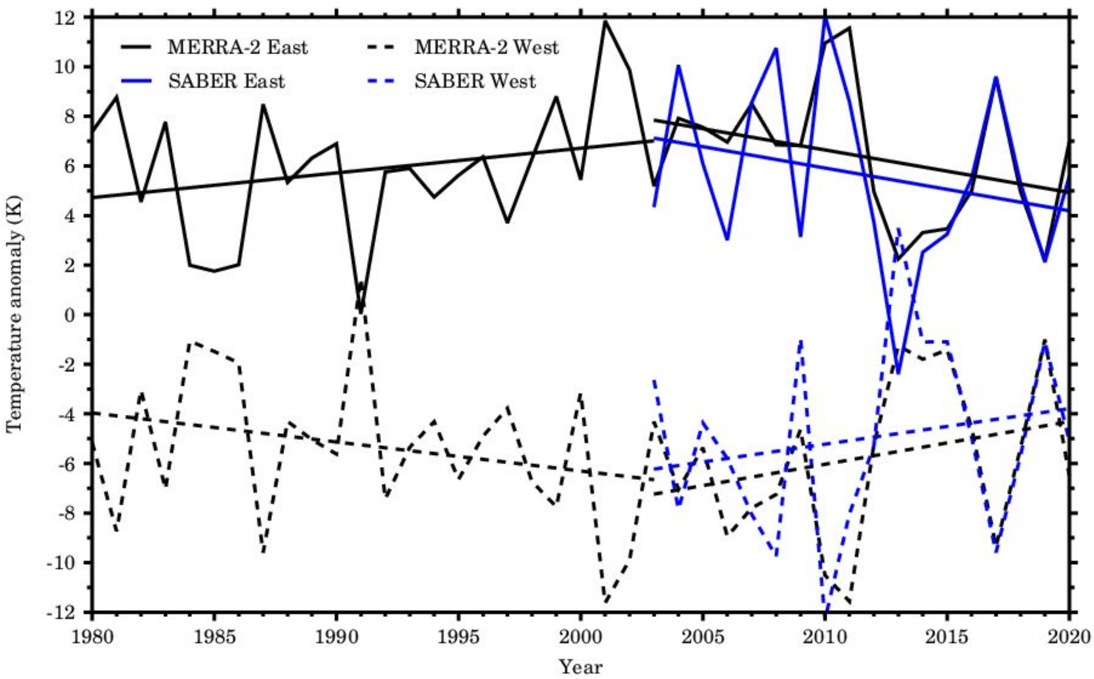

Fig. 2. Time series of the zonal temperature deviations averaged over the climatological high-temperature lobe (hereafter East) (50°N-70°N, 30°E-180°E) (solid lines) and the climatological low-temperature lobe (hereafter West) (50°N-70°N, 0-150°W) (dashed lines) at 3 hPa during January from 1980 to 2020 derived from the MERRA-2 reanalysis data (black lines) and from 2003 to 2020 TIME/SABER observations (blue lines), respectively. The straight lines represent the linear fits of the zonal temperature deviations before and after 2003, respectively.

To depict the zonally asymmetric temperature trend variations with heights, Fig. 3 shows the longitude-height cross sections of the trends in zonal temperature deviation at 70°N during January (a) from 1980 to 2003 derived from MERRA-2 reanalysis data, (b) from 2003 to 2020 derived from MERRA-2 reanalysis data, and (c) from 2003 to 2020 derived from TIMED/SABER observations. The black contours superimposed on Fig. 3 denote the climatology of the zonal temperature deviations. The climatology of the zonal temperature deviations in the upper stratosphere and lower mesosphere (hereinafter USLM) also present a zonally asymmetric pattern, with the climatological high-temperature (low-temperature) lobe mainly located in the eastern (western) hemisphere. The climatology of the zonal temperature deviations tilts westward with heights, exhibiting a pattern analogous to that of the quasi-stationary planetary wavenumber 1 (wave 1).

As shown in Fig. 3a, the trend in the zonal temperature deviation is generally in phase with the climatology of the zonal temperature deviation in the USLM, with a statistically significant warming (cooling) trend in the eastern (western) hemisphere near the stratopause before the 2000s. In contrast, Fig. 3b shows the trend in the zonal temperature deviation is generally out of phase with the climatology of the zonal temperature deviation in the USLM, with a statistically significant cooling (warming) trend mainly located in the eastern (western) hemisphere near the stratopause after the 2000s. The longitude-height cross section of the zonal temperature deviation derived from MERRA-2 reanalysis data (Fig. 3b) is comparable to that derived from TIMED/SABER observations (Fig. 3c). The results in Fig. 3 further support that the zonally asymmetric temperature trend pattern undergoes a transition in the east-west direction around the 2000s and is most pronounced near the stratopause.

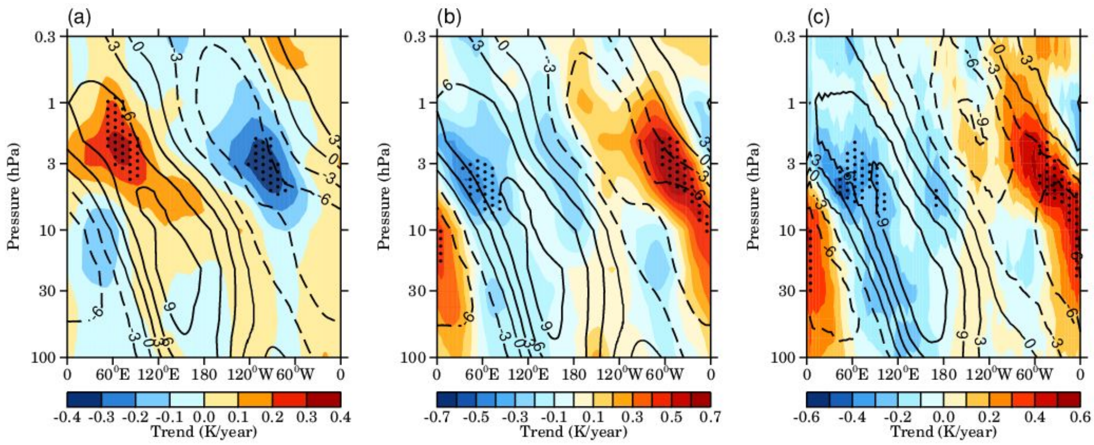

Fig. 3. Longitude-height cross sections of the trends (color shading) and climatology (black contours, the contour interval is 3 K, solid and dashed lines indicate positive and negative values, respectively) of zonal temperature deviations at 70°N during January (a) from 1980 to 2003 derived from MERRA-2 reanalysis dataset, (b) from 2003 to 2020 derived from MERRA-2 reanalysis dataset, and (c) from 2003 to 2020 derived from TIMED/SABER observations. The values over the stippled areas are statistically significant at the 95% confidence level according to Student's t test.

4. Factors Responsible for the Temperature Trends

The previous section mentioned that the zonally asymmetric temperature trends near the NH stratopause result from changes in the zonal temperature deviations and may be controlled by thermodynamic factors. France et al. (2012) reported that the advection and dissipation of quasi-stationary planetary waves could largely influence the spatial structure of temperatures at mid-high latitudes in the upper stratosphere. Therefore, the contributions of wave activities to the zonally asymmetric temperature trends are first examined here. Figs. 4a and 4d shows the latitude-height distributions of the trends in the EP flux (green vectors) and its divergence (color shading) during January from 1980 to 2003 and from 2003 to 2020 derived from MERRA-2 reanalysis

datasets, respectively. The signs of trends in EP flux are upward (downward) from the troposphere to the lower mesosphere at mid-high latitudes, indicating enhanced (weakened) wave activities throughout the troposphere and stratosphere before (after) the 2000s. In particular, the magnitudes of EP flux trends are robust in the mid-high latitude USLM, where the zonally asymmetric temperature trends exist. The negative (positive) trend in EP flux divergence is robust and statistically significant near the mid-high latitudes stratopause, supporting the enhanced (weakened) wave activities are most pronounced near the mid-high latitudes stratopause before (after) the 2000s. The trends of EP flux and its divergence in Fig. 4a are generally opposite to those in Fig. 4d, indicating the intensity of wave activities also underwent a transition around the 2000s from the troposphere to the lower mesosphere at mid-high latitudes.

According to Fig. 3, the climatology and trends of the zonal temperature deviations in the mid-high latitude USLM display a wave 1 pattern, suggesting that wave 1 activities may play a key role in modulating zonal temperature deviations. Therefore, we separate total waves into wave 1 and residual waves. Figs. 4b and 4e are the same as Figs. 4a and 4d, but for the EP flux and its divergence associated with wave 1, respectively. Figs. 4c and 4f are the same as Figs. 4a and 4d, but for the EP flux and its divergence associated with residual waves, respectively. The morphology and magnitude shown in Fig. 4b (4e) are much similar to those in Fig. 4a (Fig. 4d), confirming that the intensity of wave 1 are enhanced (weakened) before (after) the 2000s, and the changes in wave activities are dominated by changes in wave 1 activities. Besides, Fig. 4c depicts that the EP flux and its divergence associated with residual

waves do not show statistically significant changes in the USLM from 1980 to 2003. Fig. 4f presents a statistically significant negative trend in EP flux divergence in the high latitude upper stratosphere, along with the upward sign of the EP flux trend, which indicates that the intensity of residual waves is enhanced in this region from 2003 to 2020 but is contrary to that of wave 1 (Fig. 4e). The combine effects of enhanced residual waves and weakened wave 1 result in slightly weakened total waves in this region (Fig. 4d).

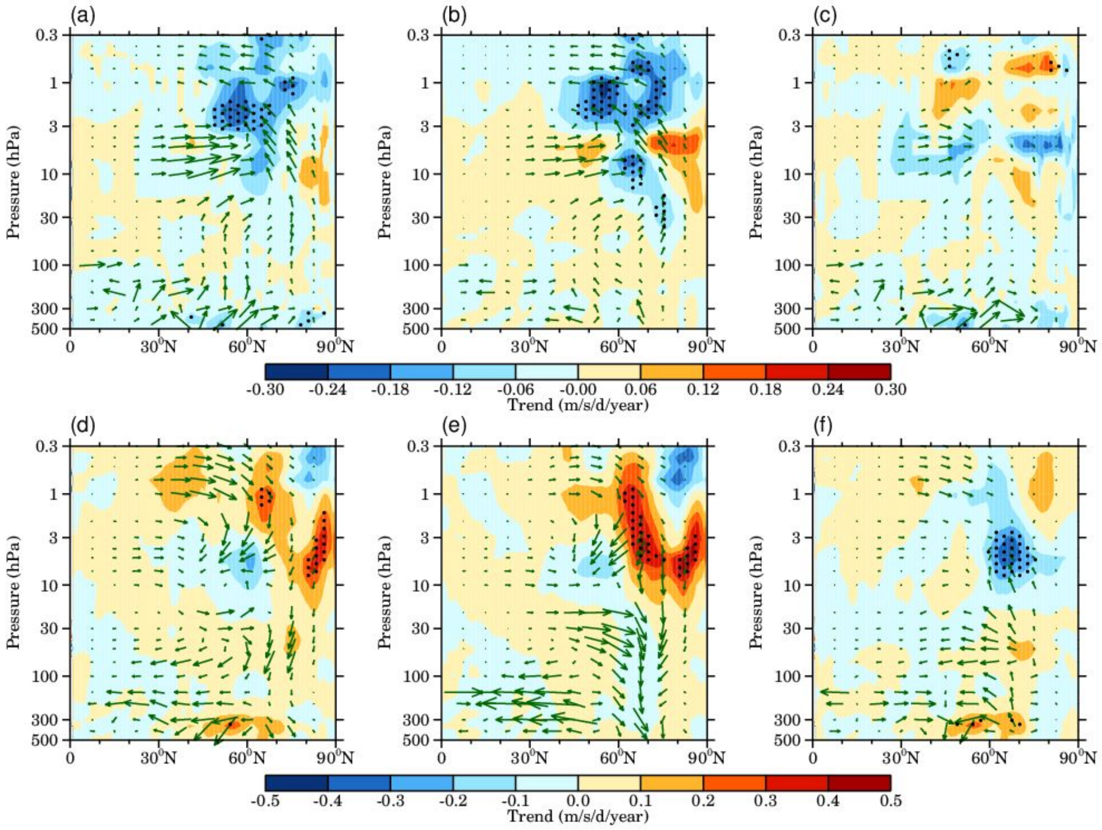

Fig. 4. (a) Latitude-height distribution of trends in Eliassen-Palm (EP) fluxes (green vectors, units in the horizontal and vertical components are 10^{-2} and 10^{-4} m^2/s^2/year, respectively) and the EP flux divergence (color shading) in January during the period from 1980 to 2003. (b) The same as (a), but for the EP flux and its divergence associated

with wave 1. (c) The same as (a), but for the EP flux and its divergence associated with residual waves. (d), (e), and (f) are the same as (a), (b), and (c), respectively, but the time period is from 2003 to 2020. The EP fluxes are multiplied by the square root of 1000/pressure (hPa). The trends over stippled areas are statistically significant at the 95% confidence level according to Student's t test. The results are derived from the MERRA-2 reanalysis dataset.

Since the changes in zonal mean wave 1 activities underwent a transition around the 2000s, which is coincident with the changes in the zonally asymmetric temperature trend patten, we further examine the zonal variations in wave 1 and the effects of wave 1 on the zonally asymmetric temperature variations. Figs. 5a and 5c present the longitude-height cross sections of the trends (color shading) and climatology (black contours) of temperature associated with wave 1 at 70°N during January from 1980 to 2003 and from 2003 to 2020 derived from the MERRA-2 reanalysis dataset, respectively. The temperature trends associated with wave 1 tilt westward with heights and are generally in phase (out of phase) with their climatology throughout the stratosphere, indicating enhanced (weakened) wave 1 activities before (after) the 2000s. In particular, the temperature trends associated with wave 1 are robust and statistically significant near the stratopause. The results in Fig. 5 are comparable to those in Fig. 3 in the USLM, indicating the changes in wave 1 are responsible for the changes in zonal temperature deviations. Moreover, Both Figs. 5a and 5c show statistically significant temperature trends associated with wave 1 in the troposphere, suggesting significant changes in the tropospheric wave 1 before and after the 2000s, respectively. The green

vectors superimposed on Figs. 5a and 5c are the trends of Plumb fluxes associated with wave 1. The signs of the trends of Plumb flux associated with wave 1 are upward (downward) from the troposphere and the lower mesosphere, which further supports enhanced (weakened) wave 1 activities from the troposphere and the lower mesosphere within the whole latitudinal band before (after) the 2000s.

Figs. 5b and 5d are the same as Figs. 5a and 5c, respectively, but for the meridional wind associated with wave 1. Likewise, the trend of the meridional wind associated with wave 1 is in phase (out of phase) with the climatology of the meridional wind associated with wave 1 from the troposphere to the lower mesosphere before (after) the 2000s. The strongest amplitude of the meridional wind associated with wave 1 is near the stratopause and dominates the meridional wind there (Andrews et al, 1987). The poleward (equatorward) meridional wind associated with wave 1 induces warm (cold) meridional temperature advection in the eastern (western) hemispheres near the stratopause, resulting in the climatological high-temperature (low-temperature) mainly located in the eastern (western) hemispheres. Since the intensity of wave 1 is strengthened (weakened) before (after) the 2000s, it enhances (reduces) the meridional temperature advection near the stratopause; consequently, the zonally asymmetric trends in zonal temperature deviations are in phase (out of phase) with their climatology near the stratopause. Gabriel et al. (2007, 2011a) also noted that the wave 1 structure of temperature near the stratopause is controlled by zonally asymmetric transport by geostrophically balanced winds.

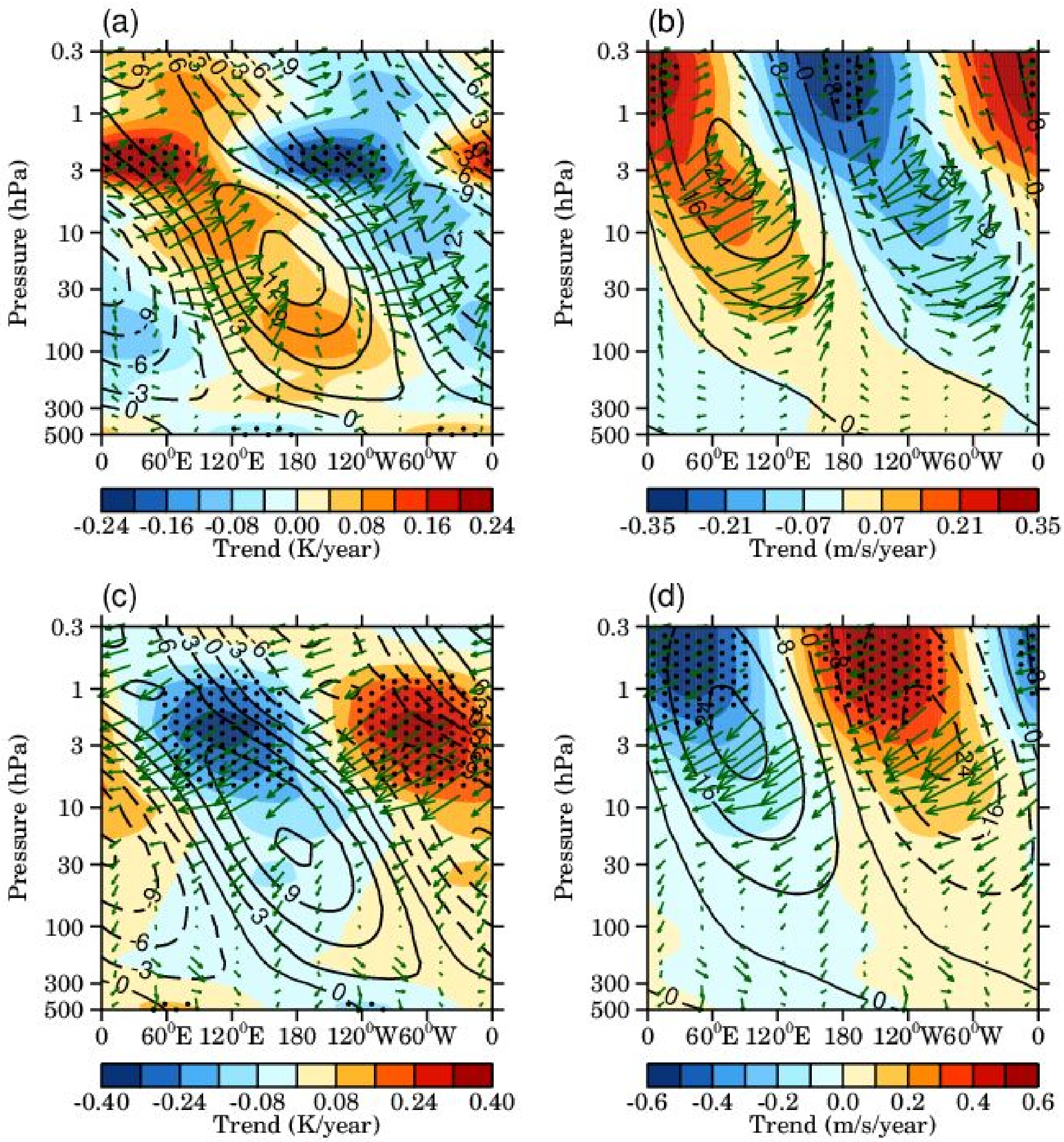

Fig. 5. Longitude-height cross sections of the trends (color shading) and climatology (black contours, the contour interval is 3 K, solid and dashed lines indicate positive and negative values, respectively) of (a) the temperature associated with wave 1 and (b) the meridional wind associated with wave 1 at 70°N from 1980 to 2003, respectively. (c) and (d) are the same as (a) and (b), respectively, but the time period is from 2003 to 2020. The green vectors denote Plumb flux trends associated with wave 1 (units in the horizontal and vertical components are 10^{-2} and 10^{-4} m^2/s^2/year, respectively). The vertical and horizontal wave fluxes are multiplied by the square root of 1000/pressure

(hPa). The stippled areas are statistically significant at the 95% confidence level according to Student's t test. The results are derived from the MERRA-2 dataset.

The long-term correlations between the zonally asymmetric temperature variations and the corresponding wave 1 component are shown in Fig. 6. The black line denotes the time series of the temperature differences between the climatology high-temperature region (50°N-70°N, 30°E-180°E) and climatology low-temperature region (50°N-70°N, 0-150°W) at 3 hPa (hereafter referred to as East–West) during January from 1980 to 2020 derived from the MERRA-2 reanalysis dataset. The red line denotes the time series of the vertical wave flux associated with wave 1 averaged between 40°N-70°N at 3 hPa (hereafter referred to as Fz1) during January from 1980 to 2020 derived from the MERRA-2 reanalysis dataset. It is seen that there is a strong correlation between wave 1 and hemispheric temperature differences near the stratopause. The correlation coefficient between Fz1 and East–West is 0.79 (0.77 when removing their linear trends), which is statistically significant at the 99% confidence level. Moreover, there is an apparent transition in the East–West (Fz1) around the 2000s, with a statistically significant increasing (decreasing) trend from 1980 to 2003 (2003 to 2020) during January. The increasing trend in East–West (Fz1) is 0.24 K/year (2.1×10^{-5} m^2/s^2/year), and the decreasing trend in East–West (Fz1) is -0.30 K/year (-2.7×10^{-5} m^2/s^2/year). Furthermore, Fz1 can explain 61% (64%) of the East–West variance and has a 60% (62%) contribution to the East–West trend from 1980 to 2003 (from 2003 to 2020) during January, as estimated from the linear regression method. Overall, the changes in the intensity of wave 1 can adequately explain the zonally asymmetric

temperature trends near the stratopause.

The East–West time series during January from 2003 to 2020 derived from TIMED/SABER observations is shown by the green line in Fig. 6. The East–West time series derived from TIMED/SABER observations agrees well with that derived from the MERRA-2 reanalysis dataset, with a 0.96 correlation coefficient.

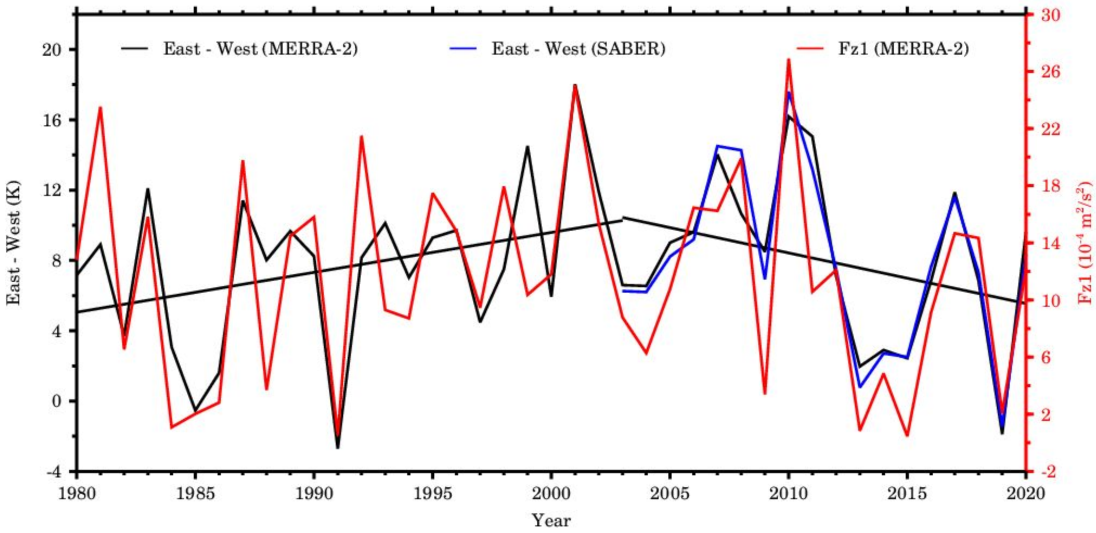

Fig. 6. Time series of the differences between the climatology of the high-temperature region (50°N-70°N, 30°E-180°E) and the climatology of the low-temperature region (50°N-70°N, 0-150°W) at 3 hPa (East–West) during January derived from the MERRA-2 reanalysis data (black line) and TIMED/SABER observations (green line), respectively, as well as the vertical wave flux associated with wave 1 (Fz1) averaged between 50°N - 70°N at 3 hPa (red line). The black straight lines are linear fits of the East–West during 1980–2003 and 2003–2020 derived from MERRA-2 reanalysis dataset.

It should be noted that the downwelling of the Brewer-Dobson circulation (BDC) may also affect the stratospheric temperature via adiabatic processes. Lin et al. (2009)

noted that enhanced BDC led to dynamic warming and produced a zonally asymmetric structure along with ozone-induced radiative cooling in the lower and middle stratosphere during September and October from 1979 to 2007. Thus, a zonally asymmetric pattern in temperature near the stratopause may be induced not only by the meridional advection of wave 1 but also by the effects of BDC. However, our analysis reveals that the residual vertical velocity in the stratosphere (i.e., the downwelling of BDC) does not have statistically significant changes, which agrees with Fu et al. (2019, Fig. 3). Therefore, the BDC contributes slightly to the zonally asymmetric temperature trends during the study period.

The intensity of the stratospheric stationary planetary waves is affected by the tropospheric wave source (e.g., Matsuno, 1970). Thus, the shift in the intensity of wave 1 near the stratopause may also induced by the shift in intensity of tropospheric wave 1 source. Figs. 7a and 7b present the spatial map of trends in 500-hPa geopotential height associated with wave 1 during January from 1980-2003 and from 2003-2020 derived from MERRA-2 reanalysis dataset, respectively. Black contour lines overlapped in Figs. 7a and 7b denote the climatology of 500-hPa geopotential height associated with wave 1. It is seen that a transition in the intensity of the tropospheric wave 1 around the 2000s. There is a statistically significant increasing (decreasing) trend in the geopotential height over the eastern European and a statistically significant decreasing (increasing) trend in the geopotential height over North Pacific at mid-high latitude before (after) the 2000s, which is generally in phase (out of phase) with the climatological eastern European high and the North Pacific low, respectively, indicating an enhanced

(weakened) wave 1 in the mid-high latitude troposphere before (after) the 2000s. Garfinkel et al. (2010) noted that the in phase (out of phase) of geopotential height anomalies in the eastern European high and the North Pacific low in the troposphere can constructively (destructively) interfere with the tropospheric wave 1 and thus enhance (weaken) the stratospheric wave 1.

Figs. 7c and 7d show the time series of the amplitude and phase anomaly of 500-hPa geopotential height associated with wave 1 at 70°N, respectively. The trend in wave 1 amplitude also underwent a transition before (1.6 m/year) and after (-1.1 m/year) the 2000s, which agrees with the results in Figs 7a and 7b. According to Smith et al. (2010), The increasing trend in phase of wave 1 before the 2000s (3.9 degree/year) and decreasing trend in phase of wave 1 after the 2000s (-3.3 degree/year), further supporting the constructively and destructively interfere with the tropospheric wave 1 before and after the 2000s, respectively.

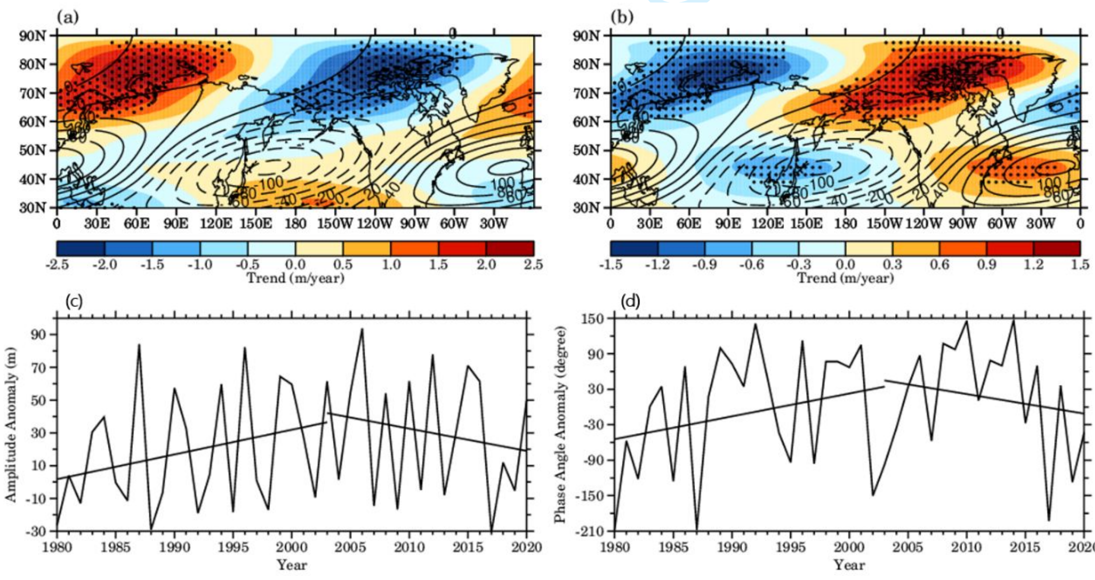

Fig. 7. (a) The spatial map of trends (color shading) and climatology (black contours, the contour interval is 20 m, solid and dashed lines indicate positive and negative values,

respectively) of 500-hPa geopotential height associated with wave 1 during January from 1980 to 2003 derived from MERRA-2 reanalysis data. (b) The same as (a), but the time period is from 2003 to 2020. The values over stippled areas are statistically significant at the 90% confidence level according to Student's t test. (c) Time series of the amplitude of 500-hPa geopotential height associated with wave 1 at 70°N. The black straight lines are linear fits of the amplitude during 1980–2003 and 2003–2020, respectively. (d) is the same as (c), but for the phase of 500-hPa geopotential height associated with wave 1.

5. Conclusions and discussion

In this study, TIMED/SABER satellite observations and the MERRA-2 reanalysis dataset were used to investigate the spatial variations in the temperature trend near the NH stratopause during January from 1980 to 2020 and the possible factors responsible for these trends. We find that there is a zonally asymmetric temperature trend pattern near the northern mid-high latitude stratopause during January. There was a warming (cooling) trend in the eastern (western) hemisphere near the stratopause before the 2000s. However, a reversed zonally asymmetric temperature trend in the east-west direction was identified after the 2000s. Although the warming trends are statistically insignificant, they contrasted with the overall cooling trend in the upper stratosphere due to ozone depletion and increasing well-mixed GHGs in recent decades. Both datasets reveal that the zonal mean temperature has an overall cooling trend during the northern winter near the stratopause. The temperature deviations from the zonal mean have similar zonally asymmetric trends and are in phase (out of phase) with the

climatology of the zonal temperature deviations before (after) the 2000s. Moreover, the zonally asymmetric trend in zonal temperature deviations tilts westward with height in the USLM and is most pronounced near the stratopause. The results derived from the MERRA-2 reanalysis dataset agree well with those derived from TIMED/SABER temperature observations in both morphology and magnitude during the TIMED/SABER satellite era.

Further analysis reveals that the meridional perturbation of wave 1 dominates the meridional wind near the stratopause, resulting in the zonally asymmetric pattern of the zonal temperature deviations. The increasing (decreasing) trend in the strength of wave 1 enhances (reduce) its meridional temperature advection near the stratopause before (after) the 2000s. Consequently, zonally asymmetric temperature trends alter in the east-west direction after (before) the 2000s. The effects of meridional temperature advection of wave 1 on the temperature in the USLM have also been reported in previous studies (e.g., Gabriel et al., 2011a). The results derived from the MERRA-2 reanalysis dataset indicate that wave 1 has a close correlation with the zonally asymmetric temperature pattern, with a statistically significant correlation coefficient of 0.79 (0.77 when removing their linear trends). The temperature variations associated with wave 1 can explain 61% (64%) of the variance in the zonally asymmetric temperature variations and contribute 60% (62%) to the zonally asymmetric temperature trend during January from 1980 to 2003 (from 2003 to 2020).

The tropospheric wave 1 at mid-high latitudes shows a strengthening (weakening) trend during January from 1980 to 2003 (from 2003 to 2020), which is in accordance

with the transition in the trend of stratospheric wave 1 intensity around the 2000s. The in phase (out of phase) of 500-hPa geopotential height anomalies in the eastern European high and the North Pacific low can constructively (destructively) interfere with the tropospheric wave 1 and thus enhance (weaken) the stratospheric wave 1 before (after) the 2000s. In addition, some studies have reported that the zonally asymmetric temperature variations near the stratopause can be modulated by 11-year solar cycles via their impact on wave 1 (Kodera and Kudora, 2002; Gabriel et al., 2011b; Liu et al., 2023). The effects of 11-year solar cycles on the zonally asymmetric temperature pattern will be investigated in future work.

Acknowledgments. We thank Han-Li Liu, William Randel, Fei Xie, Dingzhu Hu, Jiankai Zhang and Jinlong Huang for their helpful discussions and remarks. We would like to acknowledge the scientific teams at MERRA-2 and TIMED/SABER for providing the datasets.

Reference

Andrews, D. G., C. B. Leovy, and J. R. Holton, 1987: Middle atmosphere dynamics. Academic press.

Arblaster, J. M., N. P. Gillett, N. Calvo, et al., 2014: Stratospheric ozone changes and climate. *In Scientific assessment of ozone depletion: 2014.* World Meteorological Organization.

Chen, X. Y. and K. K., Tung, 2014: Varying planetary heat sink led to global-warming slowdown and acceleration. *Science*, **345**(6199), 897–903. https://doi.org/10.1126/science.1254937

Chipperfield, M. P., S. Bekki, S. Dhomse, et al., 2017: Detecting recovery of the stratospheric ozone layer. *Nature*, **549**(7671), 211-218, https://doi.org/10.1038/nature23681

Fu, Q., S. Solomon, and P. Lin, 2010: On the seasonal dependence of tropical lower-stratospheric temperature trends. *Atmospheric Chemistry & Physics*, **10**(6), 2643–2653, https://doi-org.cuucar.idm.oclc.org/10.5194/acp-10-2643-2010

Fu, Q., S. Solomon, H. A. Pahlavan, et al., 2019: Observed changes in Brewer–Dobson circulation for 1980–2018. *Environmental Research Letters*, **14**(11), 114026, doi: 10.1088/1748-9326/ab4de7

France, J. A., V. L. Harvey, C. E. Randall, et al., 2012: A climatology of stratopause temperature and height in the polar vortex and anticyclones. *Journal of Geophysical Research: Atmospheres*, **117**(D6), https://doi.org/10.1029/2011JD016893

France, J. A., and V. L. Harvey, 2013: A climatology of the stratopause in WACCM and the zonally asymmetric elevated stratopause. *Journal of Geophysical Research: Atmospheres*, **118**(5), 2241-2254, https://doi.org/10.1002/jgrd.50218

Funatsu, B. M., C. Claud, P. Keckhut, et al., 2016: Regional and seasonal stratospheric temperature trends in the last decade (2002–2014) from AMSU observations. *Journal of Geophysical Research: Atmospheres*, **121**(14), 8172-8185, https://doi.org/10.1002/2015JD024305

Golitsyn, G. S., A. I. Semenov, N. N. Shefov, et al., 1996: Long-term temperature trends in the middle and upper atmosphere, *Geophysical Research Letters*, **23**, 1741–1744, https://doi.org/10.1029/96GL01592

Gabriel, A., D. Peters, I. Kirchner, et al., 2007: Effect of zonally asymmetric ozone on stratospheric temperature and planetary wave propagation. *Geophysical Research Letters*, **34**(6), L06807, https://doi.org/10.1029/2006GL028998

Gabriel, A., H. Körnich, S. Lossow, 2011a: Zonal asymmetries in middle atmospheric ozone and water vapour derived from Odin satellite data 2001-2010. *Atmospheric Chemistry and Physics*, **11**(18), 9865-9885, https://doi-org.cuucar.idm.oclc.org/10.5194/acp-11-9865-2011

Gabriel, A., H. Schmidt, and D. H. W. Peters, 2011b: Effects of the 11-year solar cycle on middle atmospheric stationary wave patterns in temperature, ozone, and water vapor. *Journal of Geophysical Research: Atmospheres*, **116**(D23), https://doi.org/10.1029/2011JD015825

Garfinkel, C. I., D. L. Hartmann, and F. Sassi, 2010: Tropospheric precursors of anomalous Northern Hemisphere stratospheric polar vortices. *Journal of Climate*, **23**(12), 3282-3299. https://doi.org/10.1175/2010JCLI3010.1

Garcia, R. R., J. Yue, and J. M. Russell III, 2019: Middle atmosphere temperature trends in the twentieth and twenty-first centuries simulated with the Whole Atmosphere Community Climate Model (WACCM). *Journal of Geophysical Research: Space Physics*, **124**(10), 7984-7993, https://doi.org/10.1029/2019JA026909

Gelaro, R., W. McCarty, M. J. Suárez, et al., 2017: The modern-era retrospective analysis for research and applications, version 2 (MERRA-2). *Journal of climate*, **30**(14), 5419-5454, https://doi.org/10.1175/JCLI-D-16-0758.1

Harvey, V. L., and M. H. Hitchman, 1996: A climatology of the Aleutian High. *Journal*

of the atmospheric sciences, **53**(14), 2088-2102, https://doi.org/10.1175/1520-0469(1996)053<2088:ACOTAH>2.0.CO;2

Harvey, V. L., R. B. Pierce, T. D. Fairlie, et al., 2002: A climatology of stratospheric polar vortices and anticyclones. *Journal of Geophysical Research: Atmospheres*, **107**(D20), ACL-10, https://doi.org/10.1029/2001JD001471

Hu, Y., and K. K. Tung, 2002: Interannual and decadal variations of planetary wave activity, stratospheric cooling, and Northern Hemisphere annular mode. *Journal of Climate*, **15**(13), 1659-1673, https://doi.org/10.1175/1520-0442(2002)015<1659:IADVOP>2.0.CO;2

Haynes, P., 2005: Stratospheric dynamics. *Annu. Rev. Fluid Mech.*, **37**, 263-293, doi: 10.1146/annurev.fluid.37.061903.175710

Hu, Y., and Q. Fu, 2009: Stratospheric warming in Southern Hemisphere high latitudes since 1979. *Atmospheric Chemistry and Physics*, **9**(13), 4329-4340. https://doi.org/10.5194/acp-9-4329-2009

Hu, Y., Y. Xia, M. Gao, and D. Lu, 2009: Stratospheric Temperature Changes and Ozone Recovery in the 21st Century, *J. Meteor. Res.*, **23**(3), 263-275.

Hu, D., W. Tian, F. Xie et al., 2015: Impacts of stratospheric ozone depletion and recovery on wave propagation in the boreal winter stratosphere. *Journal of Geophysical Research: Atmospheres*, **120**(16), 8299-8317, https://doi.org/10.1002/2014JD022855

Hu, D., Y. Guo, and Z. Guan, 2019: Recent weakening in the stratospheric planetary wave intensity in early winter. *Geophysical Research Letters*, **46**, 3953–3962,

https://doi.org/10.1029/2019GL082113

He, Y., X. Zhu, Z. Sheng, et al., 2022: Observations of Inertia Gravity Waves in the Western Pacific and Their Characteristic in the 2015/2016 Quasi - biennial Oscillation Disruption. *Journal of Geophysical Research: Atmospheres*, **127**, e2022JD037208, https://doi.org/10.1029/2021JD034719

Ivy, D. J., S. Solomon, and H. E. Rieder, 2016: Radiative and dynamical influences on polar stratospheric temperature trends. *Journal of Climate*, **29**(13), 4927-4938. DOI: https://doi.org/10.1175/JCLI-D-15-0503.1

Kodera, K., and Y. Kuroda, 2002: Dynamical response to the solar cycle. *Journal of Geophysical Research: Atmospheres*, **107**(D24), ACL-5, https://doi.org/10.1029/2002JD002224

Keckhut, P., C. Claud, B. Funatsu, et al., 2019: Temperature trends observed in the middle atmosphere and future directions. *Infrasound Monitoring for Atmospheric Studies: Challenges in Middle Atmosphere Dynamics and Societal Benefits*, 805-823, https://doi.org/10.1007/978-3-319-75140-5_26

Lin, P., Q. Fu, S. Solomon, et al., 2009: Temperature trend patterns in Southern Hemisphere high latitudes: Novel indicators of stratospheric change. *Journal of Climate*, **22**(23), 6325-6341, https://doi.org/10.1175/2009JCLI2971.1

Long, C. S., M. Fujiwara, S. Davis, et al., 2017: Climatology and interannual variability of dynamic variables in multiple reanalysis evaluated by the SPARC Reanalysis Intercomparison Project (S-RIP), *Atmos. Chem. Phys.*, **17**, 14593–14629, https://doi.org/10.5194/acp-17-14593-2017

Liu, H. L., M. Rempel, G. Danabasuglu, et al., 2023, Climate responses under an extreme quiet sun scenario. *Journal of Geophysical Research: Atmospheres,* e2022JD037626. https://doi.org/10.1029/2022JD037626

Matsuno, T., 1970: Vertical propagation of stationary planetary waves in the winter Northern Hemisphere. *Journal of Atmospheric Sciences*, **27**(6), 871-883. https://doi.org/10.1175/1520-0469(1970)027<0871:VPOSPW>2.0.CO;2

Matsuno, T., 1971: A dynamical model of the stratospheric sudden warming. *Journal of Atmospheric Sciences*, **28**(8), 1479-1494. https://doi.org/10.1175/1520-0469(1971)028<1479:ADMOTS>2.0.CO;2

Maycock, A. C., M. M. Joshi, K. P. Shine, et al., 2014: The potential impact of changes in lower stratospheric water vapour on stratospheric temperatures over the past 30 years. *Quarterly Journal of the Royal Meteorological Society*, **140**(684), 2176–2185, https://doi.org/10.1002/qj.2287

Maycock, A. C., W. J. Randel, A. K. Steiner, et al., 2018: Revisiting the mystery of recent stratospheric temperature trends. *Geophysical Research Letters*, **45**(18), 9919-9933, https://doi.org/10.1029/2018GL078035

McLandress, C., T. G. Shepherd, A. I. Jonsson, et al., 2015: A method for merging nadir-sounding climate records, with an application to the global-mean stratospheric temperature data sets from SSU and AMSU. *Atmospheric Chemistry and Physics*, **15**, 9271-9284, https://doi.org/10.5194/acp-15-9271-2015

Plumb, R. A., 1985: On the three-dimensional propagation of stationary waves. *Journal of the Atmospheric Sciences*, **42**(3), 217-229, https://doi.org/10.1175/1520-

0469(1985)042<0217:OTTDPO>2.0.CO;2

Ramaswamy, V., M. L. Chanin, J. Angell, et al., 2001: Stratospheric temperature trends: Observations and model simulations. *Reviews of Geophysics*, **39**(1), 71-122, https://doi.org/10.1029/1999RG000065

Randel, W. J., K. P. Shine, J. Austin, et al., 2009: An update of observed stratospheric temperature trends. *Journal of Geophysical Research: Atmospheres*, **114**(D2), https://doi.org/10.1029/2008JD010421

Randel, W. J., A. K. Smith, F. Wu, et al., 2016: Stratospheric temperature trends over 1979–2015 derived from combined SSU, MLS, and SABER satellite observations. *Journal of Climate*, **29**(13), 4843-4859, https://doi.org/10.1175/JCLI-D-15-0629.1

Remsberg, E., G. Lingenfelser, V. L. Harvey, et al., 2003: On the verification of the quality of SABER temperature, geopotential height, and wind fields by comparison with Met Office assimilated analyses. *Journal of Geophysical Research: Atmospheres*, **108**(D20), 4628, https://doi.org/10.1029/2003JD003720

Remsberg, E. E., B. T. Marshall, M. Garcia-Comas, et al., 2008: Assessment of the quality of the Version 1.07 temperature-versus-pressure profiles of the middle atmosphere from TIMED/SABER. *Journal of Geophysical Research: Atmospheres*, **113**, D17101, https://doi.org/10.1029/2008JD010013

Remsberg, E., 2019: Observation and attribution of temperature trends near the stratopause from HALOE. *Journal of Geophysical Research: Atmospheres* 124.12, 6600-6611, doi: 10.1029/2019JD030455

Shine, K. P., M. S. Bourqui, P. D. F. Forster, et al., 2003: A comparison of

model-simulated trends in stratospheric temperatures. *Quarterly Journal of the Royal Meteorological Society*, **129**(590), 1565-1588, https://doi.org/10.1256/qj.02.186

Smith, K. L., C. G. Fletcher, and P. J. Kushner, 2010: The role of linear interference in the annular mode response to extratropical surface forcing. *Journal of Climate*, **23**(22), 6036-6050. https://doi.org/10.1175/2010JCLI3606.1

Seidel, D. J., N. P. Gillett, J. R. Lanzante, et al., 2011: Stratospheric temperature trends: Our evolving understanding. *Wiley Interdisciplinary Reviews: Climate Change*, **2**(4), 592-616, https://doi.org/10.1002/wcc.125

Seidel, D. J., J. Li, C. Mears, et al., 2016: Stratospheric temperature changes during the satellite era. *Journal of Geophysical Research: Atmospheres*, **121**(2), 664-681, https://doi.org/10.1002/2015JD024039

Rao, J., R. Ren, and Y. Yang, 2015: Parallel comparison of the northern winter stratospheric circulation in reanalysis and in CMIP5 models. *Advances in Atmospheric Sciences*, **32**, 952-966. https://doi.org/10.1007/s00376-014-4192-2

Steiner, A. K., F. Ladstädter, W. J. Randel, et al., 2020: Observed temperature changes in the troposphere and stratosphere from 1979 to 2018. *Journal of Climate*, **33**(19), 8165-8194. DOI: https://doi.org/10.1175/JCLI-D-19-0998.1

Thompson, D. W., and S. Solomon, 2009: Understanding recent stratospheric climate change. *Journal of Climate*, **22**(8), 1934-1943, https://doi.org/10.1175/2008JCLI2482.1

Thompson, D. W., D. J. Seidel, W. J. Randel, et al., 2012: The mystery of recent stratospheric temperature trends. *Nature*, **491**(7426), 692-697,

https://doi.org/10.1038/nature11579

Wang, L., C.-Z. Zou, and H. Qian, 2012: Construction of stratospheric temperature data records from stratospheric sounding units. *J. Climate*, **25**, 2931–2946, doi:10.1175/JCLI-D-11-00350.1.

WMO, 2018: *WMO statement on the state of the global climate in 2017*. World Meteorological Organisation, Geneva.

Xia, Y., Xu, W., Hu, Y. et al., 2020: Southern-Hemisphere high-latitude stratospheric warming revisit. Clim Dyn 54, 1671–1682. https://doi.org/10.1007/s00382-019-05083-7

Yamashita, C., H. L. Liu, and X. Chu, 2010: Gravity wave variations during the 2009 stratospheric sudden warming as revealed by ECMWF‐T799 and observations. *Geophysical Research Letters*, **37**(22), https://doi.org/10.1029/2010GL045437

Zou, C. Z., M. Gao, and M. D. Goldberg, 2009: Error structure and atmospheric temperature trends in observations from the Microwave Sounding Unit. *Journal of Climate*, **22**(7), 1661-1681, https://doi.org/10.1175/2008JCLI2233.1

Zou, C. Z., and H. Qian, 2016: Stratospheric temperature climate data record from merged SSU and AMSU-A observations. *Journal of Atmospheric and Oceanic Technology*, **33**(9), 1967-1984, https://doi.org/10.1175/JTECH-D-16-0018.1

Zhou, L., Y. Xia, and C. Zhao, 2022: Influence of Stratospheric Ozone Changes on Stratospheric Temperature Trends in Recent Decades, *Remote Sensing*, **14**(21), 5364. https://doi.org/10.3390/rs14215364

Zonally Asymmetric Temperature Trends near the Northern Middle and High Latitude Stratopause during Winter

Tao Wang[1], Wenshou Tian[1*], Ruhua Zhang[2], Jiali Luo[1], Wuhu Feng[3]

[1] *College of Atmospheric Sciences, Lanzhou University, Lanzhou* 730000*, China*

2 Department of Atmospheric and Oceanic Sciences and Institute of Atmospheric Sciences, Fudan University, Shanghai, China

[3] *NCAS, School of Earth and Environment, University of Leeds, Leeds, UK.*

(Submitted January 29, 2023)

This work is partly supported by the National Natural Science Foundation of China (42130601, 42142038).

*Corresponding author: Wenshou Tian (wstian@lzu.edu.cn). Tel: 18509486025

Abstract

The temperature trend near the stratopause is rarely evaluated owing to the limited long-term observations of global temperature. In this study, the spatial patterns of the temperature trends near the stratopause are investigated using satellite and reanalysis datasets. Our analysis reveals a zonally asymmetric temperature trend pattern near the northern mid-to-high latitude stratopause during January, and this pattern underwent an evident transition around the 2000s. From 1980 to 2003, there was a cooling trend in the western hemisphere and a warming trend in the eastern hemisphere. In contrast, a reversed zonally asymmetric temperature trend pattern existed in the east-west direction from 2003 to 2020. Although the warming trends are statistically insignificant, they contrasted with the overall cooling trend in the upper stratosphere due to ozone depletion and an increase in well-mixed greenhouse gases in recent decades. The zonally asymmetric temperature trends were induced by the transition in the intensity of quasi-stationary planetary wavenumber 1 (wave 1) near the stratopause. The increasing (decreasing) trend of the intensity of wave 1 enhanced (reduced) its meridional temperature advection near the stratopause before (after) the 2000s, consequently, a zonally asymmetric temperature trend pattern exists in the east-west direction near the stratopause. The transition in the intensity of the stratospheric wave 1 around the 2000s is most likely caused by the transition in the intensity of wave 1 activity in the troposphere.

Key words: Stratospheric temperature trend, zonally asymmetric temperature pattern, quasi-stationary planetary wavenumber 1

1. Introduction

The stratospheric temperature is a crucial climate marker that is affected by both thermal-dynamic and chemical processes. In response to ozone depletion and increasing well-mixed greenhouse gases (GHGs), the stratospheric temperature has experienced a significant cooling trend over the past several decades, which has been noted by a wide variety of observations and reproduced by multiple climate models (e.g., Golitsyn et al., 1996; Ramaswamy et al., 2001; Wang et al., 2012; Thompson et al., 2009, 2012; Randel et al., 2009, 2017; Rao et al., 2015; Garcia et al., 2019; Remsberg, 2019; Steiner et al., 2020). Notably, recently updated and extended satellite data has provided relatively reliable zonal mean temperature observations throughout the stratosphere and revealed that the zonal mean temperature trends decreased with altitude from the lower stratosphere to the upper stratosphere from 1979 to 2015 (McLandress et al., 2015; Randel et al., 2016; Zou and Qian, 2016). However, the long-term trends in stratospheric temperature still have uncertainties in both their magnitudes and spatial variations (e.g., Shine et al., 2003; Fu et al., 2010; Seidel et al., 2011; Funatsu et al., 2016; Maycock et al., 2018). These uncertainties are partly due to discrepancies in different observations (e.g., Zou et al., 2009; Thompson et al., 2012; Keckhut et al., 2019; Seidel et al., 2016) and are partly relate to the challenges involved in clarifying the factors that contribute to stratospheric temperature trends (e.g., Hu and Fu, 2009; Hu et al., 2009; Ivy et al., 2016; Xia et al., 2020; Zhou et al., 2022).

Various factors may influence temperature trends in the stratosphere. Although well-mixed GHGs are still increasing, a weak recovery signal has appeared in

stratospheric ozone in the last two decades (e.g., Hu et al., 2015; Chipperfield et al., 2017). Consequently, future trends in stratospheric temperatures (Arblaster et al., 2014; WMO, 2018) will mainly result from the opposing effects of increasing CO_2 (colder stratosphere) and increasing ozone (the warmer stratosphere). Moreover, the increasing stratospheric water vapor and volcanic aerosols have potentially impacted the temperature trends in the tropical lower stratosphere in recent decades (e.g., Maycock et al., 2014). Apart from the radiative contributions of chemical constituents, dynamic processes also have a large impact on stratospheric temperature trends, particularly at middle and high latitudes. It is known that temperatures in the stratosphere at middle and high latitudes are dominated by both the radiative balance and dynamic heating originating from tropospheric wave forcing (Andrews et al., 1987; Haynes, 2005; He et al., 2022). Given that GHGs trends are monotonically increasing, the temperature trends in the stratosphere at middle and high latitudes are strongly modulated by changes in planetary wave forcing in the stratosphere (Hu and Tung, 2002; Fu et al., 2019). As a result, the large interannual and decadal variations in dynamical forcing may lead to large uncertainties in stratospheric temperature trends (e.g., Matsuno, 1971; Yamashita et al., 2010; Long et al., 2017).

On the other hand, previous studies have mainly focused on trends in global or zonal mean temperatures in the stratosphere, but the longitudinal variations in the temperature trend in the stratosphere have rarely been evaluated. In particular, the spatial variations in the temperature trend near the stratopause are still poorly understood due to the shortage of long-term global observations there. It is well known

that the polar night jet is persistent in the Northern Hemisphere (NH) winter, indicating strong baroclinicity there (France and Harvey, 2013; Harvey et al., 2002). Harvey and Hitchman (1996) noted that the maximum longitudinal differences between the Aleutian High and the polar vortex were located near the stratopause. In addition, previous studies have reported the shift in the tropospheric and stratospheric climate around the 2000s (e.g., Chen and Tung, 2014; Hu et al., 2019). However, whether the climate shift occurs near the stratopause is still unclear. Therefore, it is of interest to investigate the changes in the temperature near the stratopause in recent decades.

In this study, we employ the Modern-Era Retrospective Analysis for Research and Applications, version 2 (MERRA-2) reanalysis datasets from 1980 to 2020 and the TIMED/SABER satellite temperature data from 2003 to 2020 to investigate spatial variations in the temperature trend near the stratopause during the northern winter as well as the possible factors responsible for the temperature trends near the stratopause. The organization of our paper is as follows. Section 2 describes the data and method we used. In Section 3, we exhibit and compare the temperature trends near the stratopause during the northern winter derived from TIMED/SABER observations and the MERRA-2 reanalysis dataset. In Section 4, we investigate possible factors responsible for the temperature trends. The conclusions and discussions are summarized in Section 5.

2. Data and Methods

2.1 Data

SABER is an infrared limb sounder launched on the TIMED satellite, which provides reliable global temperature data above the troposphere. Its latitudinal coverage ranges from a north-looking mode (53°S–83°N) to a south-looking mode (53°N–83°S) approximately every 60 days. The SABER temperature profiles have been retrieved from infrared emissions of CO_2 from approximately 16 km to 105 km altitude with an effective vertical resolution of 2 km. TIMED/SABER temperature has been evaluated by Remsberg et al. (2003, 2008). In this study, we use the TIMED/SABER (version 2.0) temperature dataset from 2003 to 2020 and bin the data into 2° × 4° (longitude by latitude) monthly mean maps.

MERRA-2 is produced by the National Aeronautics and Space Administration (NASA) Global Modeling and Assimilation Office (GMAO). The temperature data from the Microwave Limb Sounder (MLS) are assimilated in MERRA-2 above 5 hPa, providing more accurate temperature data for the upper stratosphere than MERRA (Gelaro et al. (2017). The zonal mean temperature comparisons between observations and reanalysis datasets, including MERRA-2, were investigated by Long et al. (2017). The MERRA-2 instM_3d_asm_Np monthly mean datasets (Version 5.12.4) are used during the period from 1980 to 2020, with a horizontal resolution of 0.5° × 0.625° (latitude × longitude) and 42 vertical levels up to a height of 0.1 hPa.

2.2 Method

In this study, the Eliassen-Palm (EP) flux (Andrews et al., 1987) and the Plumb flux (Plumb, 1985) are applied to measure the strength and propagation of wave activities in two dimensions and three dimensions, respectively. The meridional ($F^{(\varphi)}$) and vertical ($F^{(z)}$) components of the EP flux and its divergence ($\nabla \cdot \boldsymbol{F}$) are defined as follows:

$$F^{(\varphi)} = \rho_0 a\cos\varphi\left(\overline{u}_z\frac{\overline{v'\theta'}}{\overline{\theta}_z} - \overline{u'v'}\right) \tag{1}$$

$$F^{(z)} = \left(f - \frac{(\overline{u}\cos\varphi)_\varphi}{a\cos\varphi}\right)\frac{\overline{v'\theta'}}{\overline{\theta}_z} - \overline{u'w'} \tag{2}$$

$$\nabla\cdot\boldsymbol{F} = \frac{\partial F^{(\varphi)}}{\partial\varphi} + \frac{\partial F^{(z)}}{\partial z} \tag{3}$$

where φ is latitude, z is height, ρ is air density, a is the Earth's radius, f is the Coriolis parameter, θ is potential temperature, u is zonal wind, v is meridional wind, and w is vertical wind. The overbars and primes denote the zonal mean and the departure from the zonal mean, respectively. The subscript 0 is for the background variables. The subscript z is for the partial derivative for the variables in the vertical direction.

The longitude ($F^{(\lambda)}$), latitude ($F^{(\varphi)}$), and vertical ($F^{(z)}$) components of the Plumb flux and its divergence ($\nabla\cdot\boldsymbol{F}$) are defined as follows:

$$F^{(\lambda)} = \rho_0\cos\varphi\left(\frac{1}{2a^2\cos^2\varphi}\left[\left(\frac{\partial\psi'}{\partial\lambda}\right)^2 - \psi'\frac{\partial^2\psi'}{\partial\lambda^2}\right]\right) \tag{4}$$

$$F^{(\varphi)} = \rho_0\cos\varphi\left(\frac{1}{2a^2\cos^2\varphi}\left[\frac{\partial\psi'}{\partial\lambda}\frac{\partial\psi'}{\partial\varphi} - \psi'\frac{\partial^2\psi'}{\partial\lambda\partial\varphi}\right]\right) \tag{5}$$

$$F^{(z)} = \rho_0\cos\varphi\left(\frac{2\Omega^2\sin^2\varphi}{N^2 a\cos\varphi}\left[\frac{\partial\psi'}{\partial\lambda}\frac{\partial\psi'}{\partial z} - \psi'\frac{\partial^2\psi'}{\partial\lambda\partial z}\right]\right) \tag{6}$$

$$\nabla\cdot\boldsymbol{F} = \frac{\partial F^{(\lambda)}}{\partial\lambda} + \frac{\partial F^{(\varphi)}}{\partial\varphi} + \frac{\partial F^{(z)}}{\partial z} \tag{7}$$

where λ is longitude, Ω is the Earth's angular velocity, N is the Brunt–Väisälä frequency, $\psi = \Phi/2\Omega\sin\varphi$, and Φ is potential height.

3. Temperature Trends Near the Stratopause during the Northern Winter

Figs. 1a and 1c present the spatial patterns of the 3 hPa temperature trends over the NH during January from 1980-2003 and from 2003-2020 derived from MERRA-2 reanalysis data, respectively. A noticeable feature is that there is a zonally asymmetric pattern in temperature trends at mid-high latitudes shown in Fig. 1a, with a cooling trend in the western hemisphere and a warming trend in the eastern hemisphere. In contrast, a reversal temperature trend in the east-west direction can be noted in Fig. 1c, with a warming (cooling) trend in the western (eastern) hemisphere. Note that the results here are not sensitive to slight changes in the starting/ending year of the time series. Thompson et al. (2012) indicated that due to ozone depletion and increasing well-mixed GHGs in recent decades, the stratospheric cooling in the upper stratosphere is more robust than that in the lower-middle stratosphere. Hence, although these warming trends in Figs. 1a and 1c are statistically insignificant at the 95% confidence level, they contrast with the overall cooling trend in the upper stratosphere. To understand the unusual warming near the stratopause, we separate the temperature into two components, i.e., zonal mean and deviations from the zonal mean (hereafter zonal temperature deviations). The zonal mean temperature denotes the background field, which is dominated by chemical and radiative balances. The temperature deviations denote the disturbed field, which is largely controlled by adiabatic/diabatic thermodynamic processes.

Figs. 1b and 1d show the spatial patterns of trends in zonal temperature deviations at 3 hPa over the NH during January from 1998 to 2003 and from 2003 to 2020 derived from MERRA-2 reanalysis data, respectively. The trends in zonal temperature deviations also present zonally asymmetric patterns at mid-high latitudes, with a statistically significant cooling (warming) trend in the western (eastern) hemisphere in Fig. 1b, and a reversal temperature trend in the east-west direction in Fig. 1d. The warming (cooling) trends in the zonal temperature deviations are stronger (weaker) compared to those in the original temperature. The green counters superimposed on Figs. 1b and 1d are the climatology of the zonal temperature deviations, which are likewise zonally asymmetric at mid-high latitudes, with negative (positive) anomalies in the western (eastern) hemisphere. The climatology of the zonal temperature deviations is generally in phase (out of phase) with the trends of the zonal temperature deviations in Fig. 1b (1d), suggesting that the zonal asymmetry of temperature variations was strengthened (weakened) before (after) the 2000s, and there was a transition in the zonally asymmetric temperature trend pattern around the 2000s.

The latitudinal variations in the 3 hPa zonal mean temperature trends over the NH during January from 1980 to 2003 and from 2003 to 2020 derived from MERRA-2 reanalysis data are shown in Fig. 1g, respectively. The morphology of zonal mean temperature trend before the 2000s is similar to that after the 2000s. The zonal mean temperature trend is close to zero at lower latitudes but decreases with increasing latitudes at mid-high latitudes. Overall, the zonal mean temperature trend before/after the 2000s is cooling in the NH, which is consistent with the increase in well-mixed GHGs in recent decades. The results shown in Fig. 1 as derived from MERRA-2 reanalysis data suggest that the zonal asymmetry of the temperature trends near the stratopause is the product of changes in disturbed fields.

To further verify the trends exhibited in Fig. 1 derived from MERRA-2 reanalysis data, TIMED/SABER satellite temperature observations (from 2003-2020) are analyzed. Figs. e, f, and g (blue line) are the same as Figs. c, d, and g (red line), respectively, but the data is derived from TIMED/SABER observations. It is seen that the zonally asymmetric temperature trend pattern is also apparent in TIMED/SABER observations, and the corresponding results derived from MERRA-2 reanalysis data agree well with those derived from TIMED/SABER observations in both morphology and magnitude. Since the temperature trends near the stratopause in MERRA-2 reanalysis data are in good agreement with those from the TIMED/SABER temperature observations, the MERRA-2 dataset is utilized to investigate the possible factors responsible for the zonally asymmetric variations in the temperature. Note that the spatial pattern of 3 hPa temperature shows an almost uniform cooling trend over the NH during January from 1980 to 2020 derived from MERRA-2 reanalysis data (not shown).

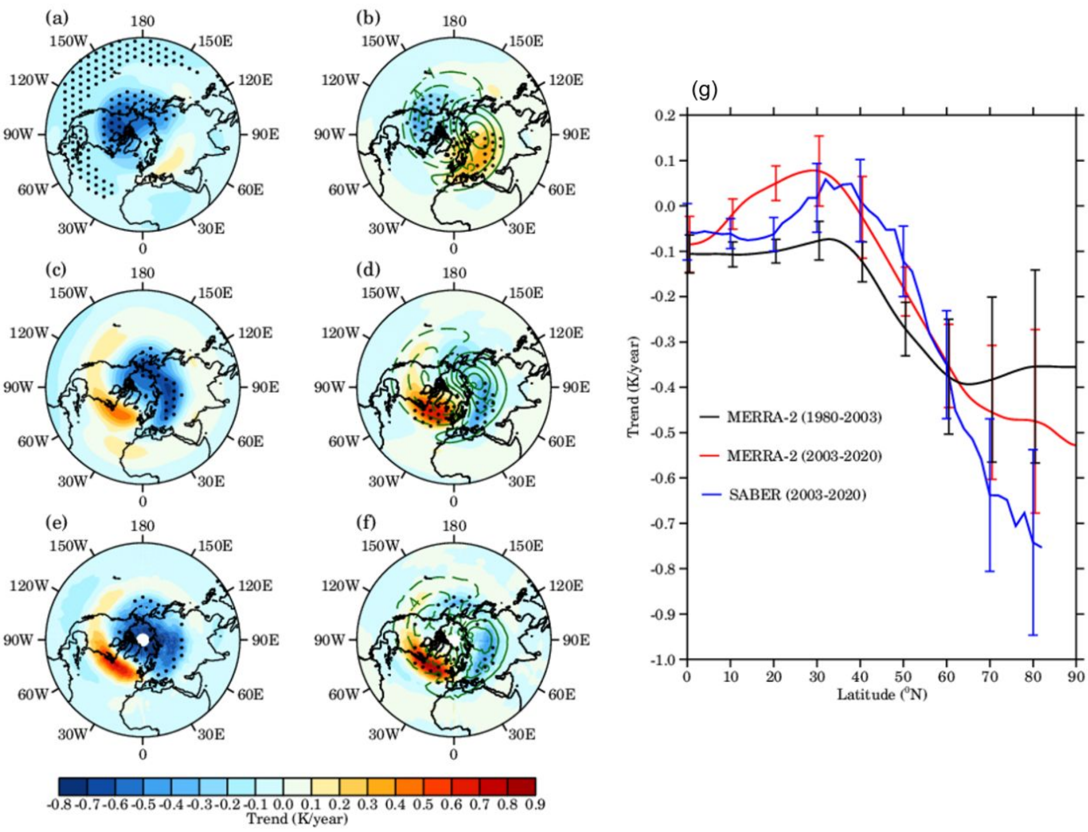

Fig. 1. Spatial pattern of trends in (a) temperature and (b) zonal temperature deviations over the NH at 3 hPa during January from 1980 to 2003 derived from MERRA-2 reanalysis data. (c) and (d) are the same as (a) and (b), respectively, but the time period is from 2003 to 2020. (e) and (f) are the same as (c) and (d), respectively, but the data is derived from TIMED/SABER observations. The values over the stippled areas are statistically significant at the 95% confidence level according to Student's t test. The green contour lines denote the climatology of the zonal temperature deviations (the contour interval is 3 K, solid and dashed lines indicate positive and negative values, respectively). (g) Latitude variations in the zonal mean temperature trends over the NH at 3 hPa during January from 1980 to 2003 derived from MERRA-2 reanalysis dataset (black line), from 2003 to 2020 derived from MERRA-2 reanalysis dataset (red line), and from 2003 to 2020 derived from TIMED/SABER observations (blue line). Error

bars show the 2σ statistical uncertainty.

Fig. 2 presents the time series of the zonal temperature deviations averaged over the climatological high-temperature lobe (hereafter East) (50°N-70°N, 30°E-180°E) (solid lines) and the climatological low-temperature lobe (hereafter West) (50°N-70°N, 0-150°W) (dashed lines) at 3 hPa during January from 1980 to 2020 derived from MERRA-2 reanalysis data (black lines) and from 2003 to 2020 derived from TIME/SABER observations (blue lines), respectively. The straight lines represent the linear fits of the zonal temperature deviations before and after 2003, respectively. The time series of the zonal temperature deviations derived from MERRA-2 agree well with those derived from the TIMED/SABER observations in both magnitudes and variations. The East underwent a statistically significant increasing trend (0.1 K/year) from 1980 to 2003 and a statistically significant decreasing trend (-0.17 K/year) from 2003 to 2020. The West has similar magnitudes but opposite signs in both interannual variations and long-term trends compared to the East, indicating a close negative correlation in the zonal temperature deviations between the two lobes. The correlation coefficients between the East and West are -0.89 (-0.90) derived from the MERRA-2 reanalysis data (TIMED/SABER observations). Note that the results here are not sensitive to slight changes in the latitude/longitude bounds used for averaging the data.

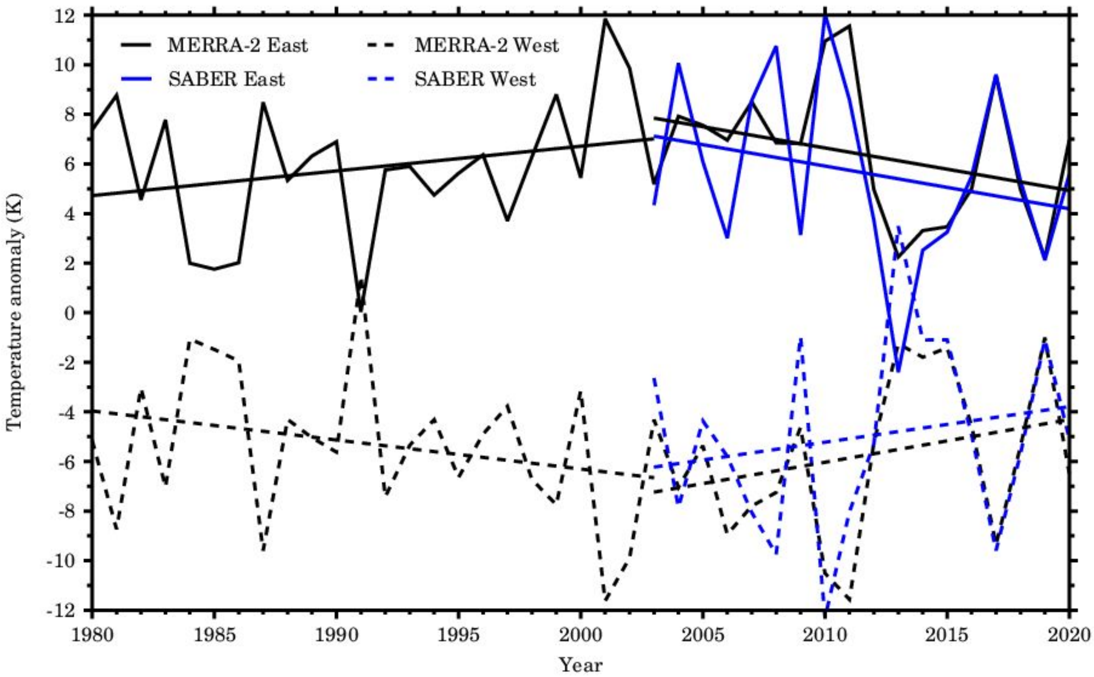

Fig. 2. Time series of the zonal temperature deviations averaged over the climatological high-temperature lobe (hereafter East) (50°N-70°N, 30°E-180°E) (solid lines) and the climatological low-temperature lobe (hereafter West) (50°N-70°N, 0-150°W) (dashed lines) at 3 hPa during January from 1980 to 2020 derived from the MERRA-2 reanalysis data (black lines) and from 2003 to 2020 TIME/SABER observations (blue lines), respectively. The straight lines represent the linear fits of the zonal temperature deviations before and after 2003, respectively.

To depict the zonally asymmetric temperature trend variations with heights, Fig. 3 shows the longitude-height cross sections of the trends in zonal temperature deviation at 70°N during January (a) from 1980 to 2003 derived from MERRA-2 reanalysis data, (b) from 2003 to 2020 derived from MERRA-2 reanalysis data, and (c) from 2003 to 2020 derived from TIMED/SABER observations. The black contours superimposed on Fig. 3 denote the climatology of the zonal temperature deviations. The climatology of the zonal temperature deviations in the upper stratosphere and lower mesosphere (hereinafter USLM) also present a zonally asymmetric pattern, with the climatological high-temperature (low-temperature) lobe mainly located in the eastern (western) hemisphere. The climatology of the zonal temperature deviations tilts westward with heights, exhibiting a pattern analogous to that of the quasi-stationary planetary wavenumber 1 (wave 1).

As shown in Fig. 3a, the trend in the zonal temperature deviation is generally in phase with the climatology of the zonal temperature deviation in the USLM, with a statistically significant warming (cooling) trend in the eastern (western) hemisphere near the stratopause before the 2000s. In contrast, Fig. 3b shows the trend in the zonal temperature deviation is generally out of phase with the climatology of the zonal temperature deviation in the USLM, with a statistically significant cooling (warming) trend mainly located in the eastern (western) hemisphere near the stratopause after the 2000s. The longitude-height cross section of the zonal temperature deviation derived from MERRA-2 reanalysis data (Fig. 3b) is comparable to that derived from TIMED/SABER observations (Fig. 3c). The results in Fig. 3 further support that the zonally asymmetric temperature trend pattern undergoes a transition in the east-west direction around the 2000s and is most pronounced near the stratopause.

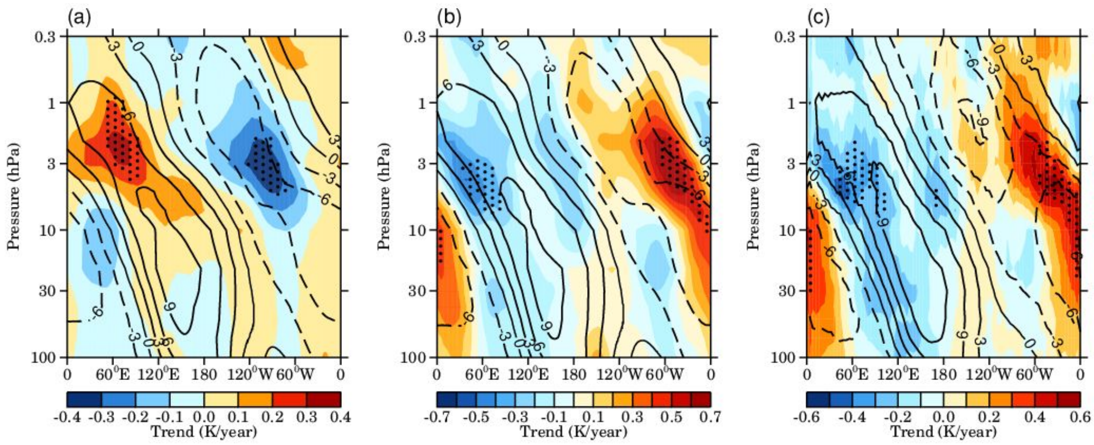

Fig. 3. Longitude-height cross sections of the trends (color shading) and climatology (black contours, the contour interval is 3 K, solid and dashed lines indicate positive and negative values, respectively) of zonal temperature deviations at 70°N during January (a) from 1980 to 2003 derived from MERRA-2 reanalysis dataset, (b) from 2003 to 2020 derived from MERRA-2 reanalysis dataset, and (c) from 2003 to 2020 derived from TIMED/SABER observations. The values over the stippled areas are statistically significant at the 95% confidence level according to Student's t test.

4. Factors Responsible for the Temperature Trends

The previous section mentioned that the zonally asymmetric temperature trends near the NH stratopause result from changes in the zonal temperature deviations and may be controlled by thermodynamic factors. France et al. (2012) reported that the advection and dissipation of quasi-stationary planetary waves could largely influence the spatial structure of temperatures at mid-high latitudes in the upper stratosphere. Therefore, the contributions of wave activities to the zonally asymmetric temperature trends are first examined here. Figs. 4a and 4d shows the latitude-height distributions of the trends in the EP flux (green vectors) and its divergence (color shading) during January from 1980 to 2003 and from 2003 to 2020 derived from MERRA-2 reanalysis

datasets, respectively. The signs of trends in EP flux are upward (downward) from the troposphere to the lower mesosphere at mid-high latitudes, indicating enhanced (weakened) wave activities throughout the troposphere and stratosphere before (after) the 2000s. In particular, the magnitudes of EP flux trends are robust in the mid-high latitude USLM, where the zonally asymmetric temperature trends exist. The negative (positive) trend in EP flux divergence is robust and statistically significant near the mid-high latitudes stratopause, supporting the enhanced (weakened) wave activities are most pronounced near the mid-high latitudes stratopause before (after) the 2000s. The trends of EP flux and its divergence in Fig. 4a are generally opposite to those in Fig. 4d, indicating the intensity of wave activities also underwent a transition around the 2000s from the troposphere to the lower mesosphere at mid-high latitudes.

According to Fig. 3, the climatology and trends of the zonal temperature deviations in the mid-high latitude USLM display a wave 1 pattern, suggesting that wave 1 activities may play a key role in modulating zonal temperature deviations. Therefore, we separate total waves into wave 1 and residual waves. Figs. 4b and 4e are the same as Figs. 4a and 4d, but for the EP flux and its divergence associated with wave 1, respectively. Figs. 4c and 4f are the same as Figs. 4a and 4d, but for the EP flux and its divergence associated with residual waves, respectively. The morphology and magnitude shown in Fig. 4b (4e) are much similar to those in Fig. 4a (Fig. 4d), confirming that the intensity of wave 1 are enhanced (weakened) before (after) the 2000s, and the changes in wave activities are dominated by changes in wave 1 activities. Besides, Fig. 4c depicts that the EP flux and its divergence associated with residual

waves do not show statistically significant changes in the USLM from 1980 to 2003. Fig. 4f presents a statistically significant negative trend in EP flux divergence in the high latitude upper stratosphere, along with the upward sign of the EP flux trend, which indicates that the intensity of residual waves is enhanced in this region from 2003 to 2020 but is contrary to that of wave 1 (Fig. 4e). The combine effects of enhanced residual waves and weakened wave 1 result in slightly weakened total waves in this region (Fig. 4d).

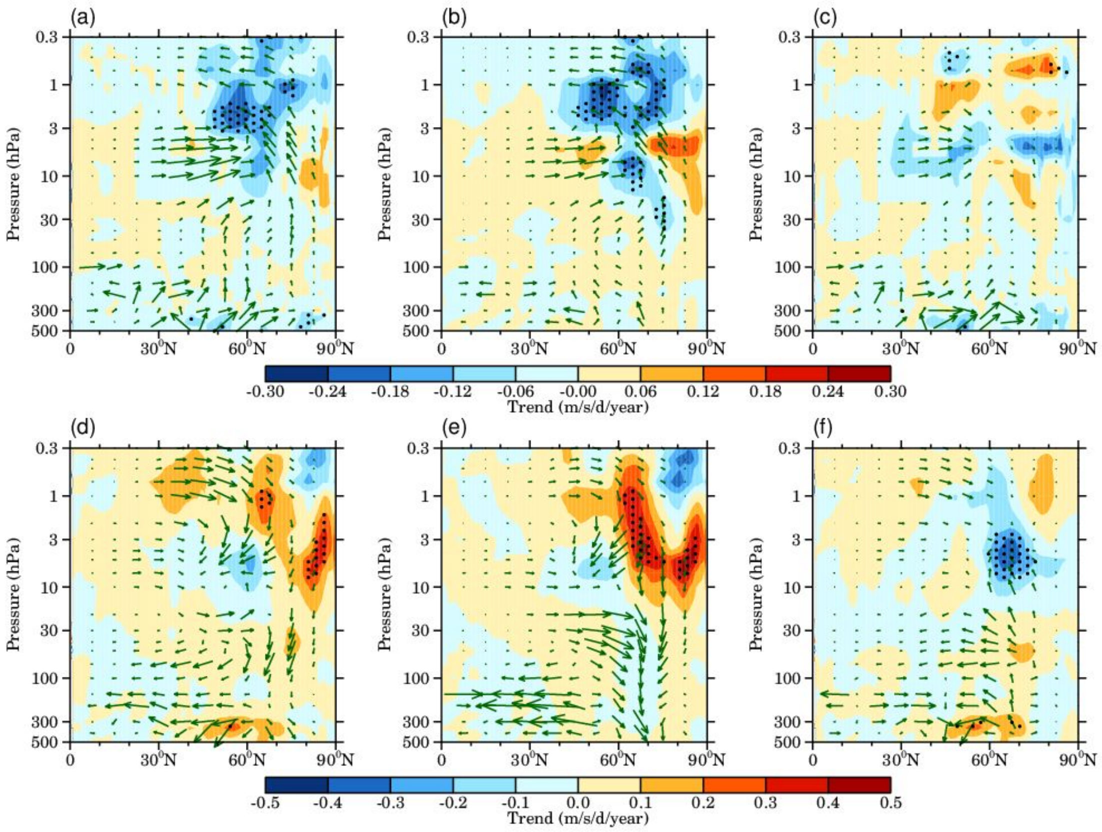

Fig. 4. (a) Latitude-height distribution of trends in Eliassen-Palm (EP) fluxes (green vectors, units in the horizontal and vertical components are 10^{-2} and 10^{-4} m^2/s^2/year, respectively) and the EP flux divergence (color shading) in January during the period from 1980 to 2003. (b) The same as (a), but for the EP flux and its divergence associated

with wave 1. (c) The same as (a), but for the EP flux and its divergence associated with residual waves. (d), (e), and (f) are the same as (a), (b), and (c), respectively, but the time period is from 2003 to 2020. The EP fluxes are multiplied by the square root of 1000/pressure (hPa). The trends over stippled areas are statistically significant at the 95% confidence level according to Student's t test. The results are derived from the MERRA-2 reanalysis dataset.

Since the changes in zonal mean wave 1 activities underwent a transition around the 2000s, which is coincident with the changes in the zonally asymmetric temperature trend patten, we further examine the zonal variations in wave 1 and the effects of wave 1 on the zonally asymmetric temperature variations. Figs. 5a and 5c present the longitude-height cross sections of the trends (color shading) and climatology (black contours) of temperature associated with wave 1 at 70°N during January from 1980 to 2003 and from 2003 to 2020 derived from the MERRA-2 reanalysis dataset, respectively. The temperature trends associated with wave 1 tilt westward with heights and are generally in phase (out of phase) with their climatology throughout the stratosphere, indicating enhanced (weakened) wave 1 activities before (after) the 2000s. In particular, the temperature trends associated with wave 1 are robust and statistically significant near the stratopause. The results in Fig. 5 are comparable to those in Fig. 3 in the USLM, indicating the changes in wave 1 are responsible for the changes in zonal temperature deviations. Moreover, Both Figs. 5a and 5c show statistically significant temperature trends associated with wave 1 in the troposphere, suggesting significant changes in the tropospheric wave 1 before and after the 2000s, respectively. The green

vectors superimposed on Figs. 5a and 5c are the trends of Plumb fluxes associated with wave 1. The signs of the trends of Plumb flux associated with wave 1 are upward (downward) from the troposphere and the lower mesosphere, which further supports enhanced (weakened) wave 1 activities from the troposphere and the lower mesosphere within the whole latitudinal band before (after) the 2000s.

Figs. 5b and 5d are the same as Figs. 5a and 5c, respectively, but for the meridional wind associated with wave 1. Likewise, the trend of the meridional wind associated with wave 1 is in phase (out of phase) with the climatology of the meridional wind associated with wave 1 from the troposphere to the lower mesosphere before (after) the 2000s. The strongest amplitude of the meridional wind associated with wave 1 is near the stratopause and dominates the meridional wind there (Andrews et al, 1987). The poleward (equatorward) meridional wind associated with wave 1 induces warm (cold) meridional temperature advection in the eastern (western) hemispheres near the stratopause, resulting in the climatological high-temperature (low-temperature) mainly located in the eastern (western) hemispheres. Since the intensity of wave 1 is strengthened (weakened) before (after) the 2000s, it enhances (reduces) the meridional temperature advection near the stratopause; consequently, the zonally asymmetric trends in zonal temperature deviations are in phase (out of phase) with their climatology near the stratopause. Gabriel et al. (2007, 2011a) also noted that the wave 1 structure of temperature near the stratopause is controlled by zonally asymmetric transport by geostrophically balanced winds.

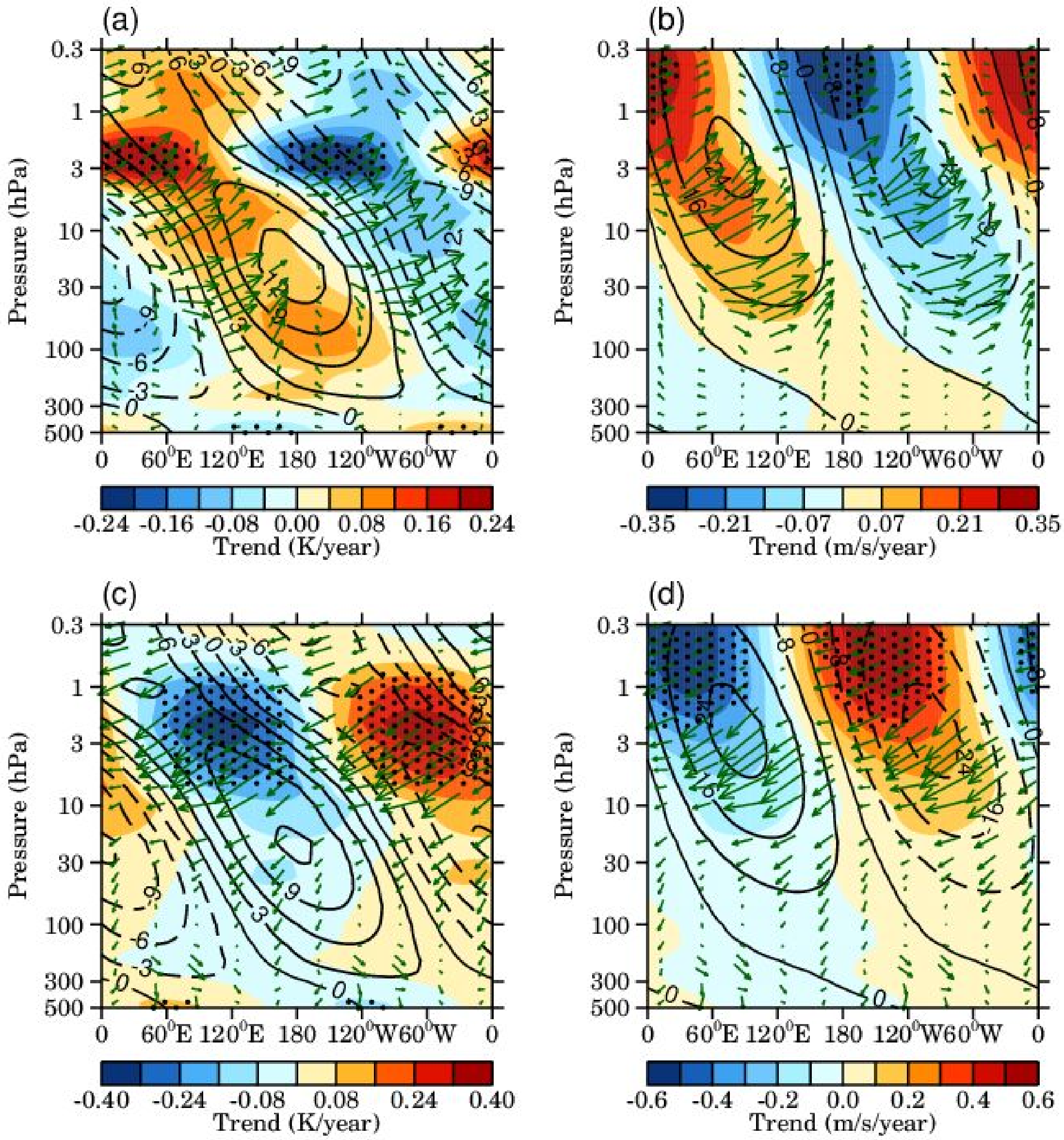

Fig. 5. Longitude-height cross sections of the trends (color shading) and climatology (black contours, the contour interval is 3 K, solid and dashed lines indicate positive and negative values, respectively) of (a) the temperature associated with wave 1 and (b) the meridional wind associated with wave 1 at 70°N from 1980 to 2003, respectively. (c) and (d) are the same as (a) and (b), respectively, but the time period is from 2003 to 2020. The green vectors denote Plumb flux trends associated with wave 1 (units in the horizontal and vertical components are 10^{-2} and 10^{-4} m^2/s^2/year, respectively). The vertical and horizontal wave fluxes are multiplied by the square root of 1000/pressure

(hPa). The stippled areas are statistically significant at the 95% confidence level according to Student's t test. The results are derived from the MERRA-2 dataset.

The long-term correlations between the zonally asymmetric temperature variations and the corresponding wave 1 component are shown in Fig. 6. The black line denotes the time series of the temperature differences between the climatology high-temperature region (50°N-70°N, 30°E-180°E) and climatology low-temperature region (50°N-70°N, 0-150°W) at 3 hPa (hereafter referred to as East–West) during January from 1980 to 2020 derived from the MERRA-2 reanalysis dataset. The red line denotes the time series of the vertical wave flux associated with wave 1 averaged between 40°N-70°N at 3 hPa (hereafter referred to as Fz1) during January from 1980 to 2020 derived from the MERRA-2 reanalysis dataset. It is seen that there is a strong correlation between wave 1 and hemispheric temperature differences near the stratopause. The correlation coefficient between Fz1 and East–West is 0.79 (0.77 when removing their linear trends), which is statistically significant at the 99% confidence level. Moreover, there is an apparent transition in the East–West (Fz1) around the 2000s, with a statistically significant increasing (decreasing) trend from 1980 to 2003 (2003 to 2020) during January. The increasing trend in East–West (Fz1) is 0.24 K/year (2.1×10^{-5} m^2/s^2/year), and the decreasing trend in East–West (Fz1) is -0.30 K/year (-2.7×10^{-5} m^2/s^2/year). Furthermore, Fz1 can explain 61% (64%) of the East–West variance and has a 60% (62%) contribution to the East–West trend from 1980 to 2003 (from 2003 to 2020) during January, as estimated from the linear regression method. Overall, the changes in the intensity of wave 1 can adequately explain the zonally asymmetric

temperature trends near the stratopause.

The East–West time series during January from 2003 to 2020 derived from TIMED/SABER observations is shown by the green line in Fig. 6. The East–West time series derived from TIMED/SABER observations agrees well with that derived from the MERRA-2 reanalysis dataset, with a 0.96 correlation coefficient.

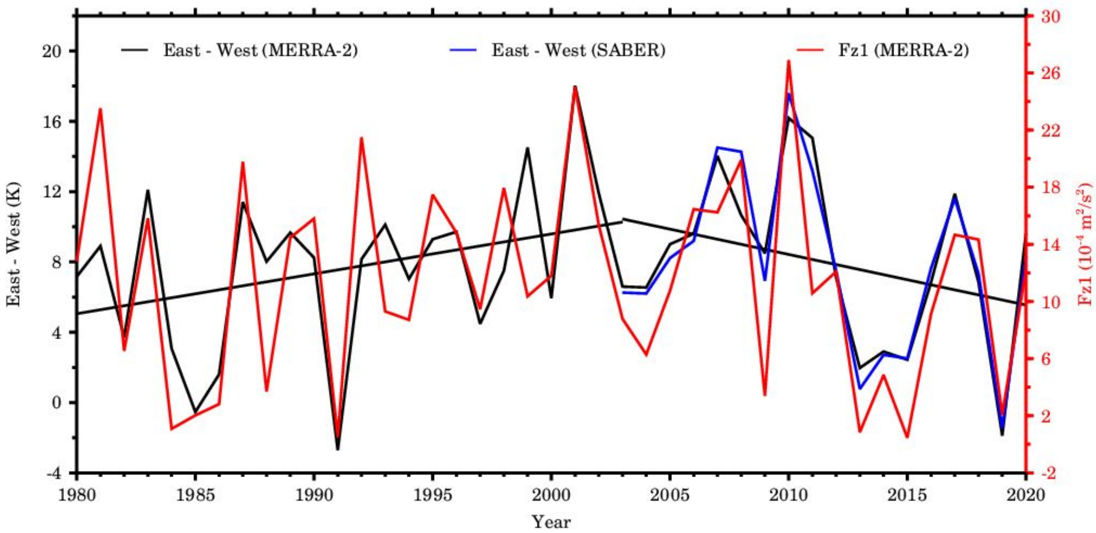

Fig. 6. Time series of the differences between the climatology of the high-temperature region (50°N-70°N, 30°E-180°E) and the climatology of the low-temperature region (50°N-70°N, 0-150°W) at 3 hPa (East–West) during January derived from the MERRA-2 reanalysis data (black line) and TIMED/SABER observations (green line), respectively, as well as the vertical wave flux associated with wave 1 (Fz1) averaged between 50°N - 70°N at 3 hPa (red line). The black straight lines are linear fits of the East–West during 1980–2003 and 2003–2020 derived from MERRA-2 reanalysis dataset.

It should be noted that the downwelling of the Brewer-Dobson circulation (BDC) may also affect the stratospheric temperature via adiabatic processes. Lin et al. (2009)

noted that enhanced BDC led to dynamic warming and produced a zonally asymmetric structure along with ozone-induced radiative cooling in the lower and middle stratosphere during September and October from 1979 to 2007. Thus, a zonally asymmetric pattern in temperature near the stratopause may be induced not only by the meridional advection of wave 1 but also by the effects of BDC. However, our analysis reveals that the residual vertical velocity in the stratosphere (i.e., the downwelling of BDC) does not have statistically significant changes, which agrees with Fu et al. (2019, Fig. 3). Therefore, the BDC contributes slightly to the zonally asymmetric temperature trends during the study period.

The intensity of the stratospheric stationary planetary waves is affected by the tropospheric wave source (e.g., Matsuno, 1970). Thus, the shift in the intensity of wave 1 near the stratopause may also induced by the shift in intensity of tropospheric wave 1 source. Figs. 7a and 7b present the spatial map of trends in 500-hPa geopotential height associated with wave 1 during January from 1980-2003 and from 2003-2020 derived from MERRA-2 reanalysis dataset, respectively. Black contour lines overlapped in Figs. 7a and 7b denote the climatology of 500-hPa geopotential height associated with wave 1. It is seen that a transition in the intensity of the tropospheric wave 1 around the 2000s. There is a statistically significant increasing (decreasing) trend in the geopotential height over the eastern European and a statistically significant decreasing (increasing) trend in the geopotential height over North Pacific at mid-high latitude before (after) the 2000s, which is generally in phase (out of phase) with the climatological eastern European high and the North Pacific low, respectively, indicating an enhanced

(weakened) wave 1 in the mid-high latitude troposphere before (after) the 2000s. Garfinkel et al. (2010) noted that the in phase (out of phase) of geopotential height anomalies in the eastern European high and the North Pacific low in the troposphere can constructively (destructively) interfere with the tropospheric wave 1 and thus enhance (weaken) the stratospheric wave 1.

Figs. 7c and 7d show the time series of the amplitude and phase anomaly of 500-hPa geopotential height associated with wave 1 at 70°N, respectively. The trend in wave 1 amplitude also underwent a transition before (1.6 m/year) and after (-1.1 m/year) the 2000s, which agrees with the results in Figs 7a and 7b. According to Smith et al. (2010), The increasing trend in phase of wave 1 before the 2000s (3.9 degree/year) and decreasing trend in phase of wave 1 after the 2000s (-3.3 degree/year), further supporting the constructively and destructively interfere with the tropospheric wave 1 before and after the 2000s, respectively.

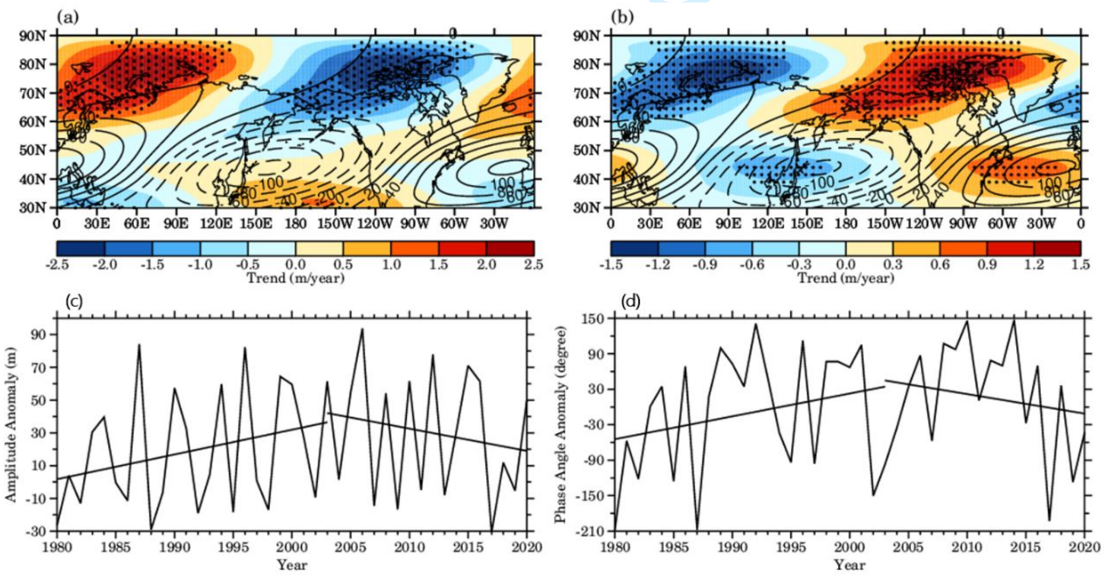

Fig. 7. (a) The spatial map of trends (color shading) and climatology (black contours, the contour interval is 20 m, solid and dashed lines indicate positive and negative values,

respectively) of 500-hPa geopotential height associated with wave 1 during January from 1980 to 2003 derived from MERRA-2 reanalysis data. (b) The same as (a), but the time period is from 2003 to 2020. The values over stippled areas are statistically significant at the 90% confidence level according to Student's t test. (c) Time series of the amplitude of 500-hPa geopotential height associated with wave 1 at 70°N. The black straight lines are linear fits of the amplitude during 1980–2003 and 2003–2020, respectively. (d) is the same as (c), but for the phase of 500-hPa geopotential height associated with wave 1.

5. Conclusion and Discussion

In this study, TIMED/SABER satellite observations and the MERRA-2 reanalysis dataset were used to investigate the spatial variations in the temperature trend near the NH stratopause during January from 1980 to 2020 and the possible factors responsible for these trends. We find that there is a zonally asymmetric temperature trend pattern near the northern mid-high latitude stratopause during January. There was a warming (cooling) trend in the eastern (western) hemisphere near the stratopause before the 2000s. However, a reversed zonally asymmetric temperature trend in the east-west direction was identified after the 2000s. Although the warming trends are statistically insignificant, they contrasted with the overall cooling trend in the upper stratosphere due to ozone depletion and increasing well-mixed GHGs in recent decades. Both datasets reveal that the zonal mean temperature has an overall cooling trend during the northern winter near the stratopause. The temperature deviations from the zonal mean have similar zonally asymmetric trends and are in phase (out of phase) with the

climatology of the zonal temperature deviations before (after) the 2000s. Moreover, the zonally asymmetric trend in zonal temperature deviations tilts westward with height in the USLM and is most pronounced near the stratopause. The results derived from the MERRA-2 reanalysis dataset agree well with those derived from TIMED/SABER temperature observations in both morphology and magnitude during the TIMED/SABER satellite era.

Further analysis reveals that the meridional perturbation of wave 1 dominates the meridional wind near the stratopause, resulting in the zonally asymmetric pattern of the zonal temperature deviations. The increasing (decreasing) trend in the strength of wave 1 enhances (reduce) its meridional temperature advection near the stratopause before (after) the 2000s. Consequently, zonally asymmetric temperature trends alter in the east-west direction after (before) the 2000s. The effects of meridional temperature advection of wave 1 on the temperature in the USLM have also been reported in previous studies (e.g., Gabriel et al., 2011a). The results derived from the MERRA-2 reanalysis dataset indicate that wave 1 has a close correlation with the zonally asymmetric temperature pattern, with a statistically significant correlation coefficient of 0.79 (0.77 when removing their linear trends). The temperature variations associated with wave 1 can explain 61% (64%) of the variance in the zonally asymmetric temperature variations and contribute 60% (62%) to the zonally asymmetric temperature trend during January from 1980 to 2003 (from 2003 to 2020).

The tropospheric wave 1 at mid-high latitudes shows a strengthening (weakening) trend during January from 1980 to 2003 (from 2003 to 2020), which is in accordance

with the transition in the trend of stratospheric wave 1 intensity around the 2000s. The in phase (out of phase) of 500-hPa geopotential height anomalies in the eastern European high and the North Pacific low can constructively (destructively) interfere with the tropospheric wave 1 and thus enhance (weaken) the stratospheric wave 1 before (after) the 2000s. In addition, some studies have reported that the zonally asymmetric temperature variations near the stratopause can be modulated by 11-year solar cycles via their impact on wave 1 (Kodera and Kudora, 2002; Gabriel et al., 2011b; Liu et al., 2023). The effects of 11-year solar cycles on the zonally asymmetric temperature pattern will be investigated in future work.

Acknowledgments. We thank Han-Li Liu, William Randel, Fei Xie, Dingzhu Hu, Jiankai Zhang and Jinlong Huang for their helpful discussions and remarks. We would like to acknowledge the scientific teams at MERRA-2 and TIMED/SABER for providing the datasets.

Reference

Andrews, D. G., C. B. Leovy, and J. R. Holton, 1987: Middle atmosphere dynamics. Academic press.

Arblaster, J. M., N. P. Gillett, N. Calvo, et al., 2014: Stratospheric ozone changes and climate. *In Scientific assessment of ozone depletion: 2014.* World Meteorological Organization.

Chen, X. Y. and K. K., Tung, 2014: Varying planetary heat sink led to global-warming slowdown and acceleration. *Science*, **345**(6199), 897–903. https://doi.org/10.1126/science.1254937

Chipperfield, M. P., S. Bekki, S. Dhomse, et al., 2017: Detecting recovery of the stratospheric ozone layer. *Nature*, **549**(7671), 211-218, https://doi.org/10.1038/nature23681

Fu, Q., S. Solomon, and P. Lin, 2010: On the seasonal dependence of tropical lower-stratospheric temperature trends. *Atmospheric Chemistry & Physics*, **10**(6), 2643–2653, https://doi-org.cuucar.idm.oclc.org/10.5194/acp-10-2643-2010

Fu, Q., S. Solomon, H. A. Pahlavan, et al., 2019: Observed changes in Brewer–Dobson circulation for 1980–2018. *Environmental Research Letters*, **14**(11), 114026, doi: 10.1088/1748-9326/ab4de7

France, J. A., V. L. Harvey, C. E. Randall, et al., 2012: A climatology of stratopause temperature and height in the polar vortex and anticyclones. *Journal of Geophysical Research: Atmospheres*, **117**(D6), https://doi.org/10.1029/2011JD016893

France, J. A., and V. L. Harvey, 2013: A climatology of the stratopause in WACCM and the zonally asymmetric elevated stratopause. *Journal of Geophysical Research: Atmospheres*, **118**(5), 2241-2254, https://doi.org/10.1002/jgrd.50218

Funatsu, B. M., C. Claud, P. Keckhut, et al., 2016: Regional and seasonal stratospheric temperature trends in the last decade (2002–2014) from AMSU observations. *Journal of Geophysical Research: Atmospheres*, **121**(14), 8172-8185, https://doi.org/10.1002/2015JD024305

Golitsyn, G. S., A. I. Semenov, N. N. Shefov, et al., 1996: Long-term temperature trends in the middle and upper atmosphere, *Geophysical Research Letters*, **23**, 1741–1744, https://doi.org/10.1029/96GL01592

Gabriel, A., D. Peters, I. Kirchner, et al., 2007: Effect of zonally asymmetric ozone on stratospheric temperature and planetary wave propagation. *Geophysical Research Letters*, **34**(6), L06807, https://doi.org/10.1029/2006GL028998

Gabriel, A., H. Körnich, S. Lossow, 2011a: Zonal asymmetries in middle atmospheric ozone and water vapour derived from Odin satellite data 2001-2010. *Atmospheric Chemistry and Physics*, **11**(18), 9865-9885, https://doi-org.cuucar.idm.oclc.org/10.5194/acp-11-9865-2011

Gabriel, A., H. Schmidt, and D. H. W. Peters, 2011b: Effects of the 11-year solar cycle on middle atmospheric stationary wave patterns in temperature, ozone, and water vapor. *Journal of Geophysical Research: Atmospheres*, **116**(D23), https://doi.org/10.1029/2011JD015825

Garfinkel, C. I., D. L. Hartmann, and F. Sassi, 2010: Tropospheric precursors of anomalous Northern Hemisphere stratospheric polar vortices. *Journal of Climate*, **23**(12), 3282-3299. https://doi.org/10.1175/2010JCLI3010.1

Garcia, R. R., J. Yue, and J. M. Russell III, 2019: Middle atmosphere temperature trends in the twentieth and twenty‐first centuries simulated with the Whole Atmosphere Community Climate Model (WACCM). *Journal of Geophysical Research: Space Physics*, **124**(10), 7984-7993, https://doi.org/10.1029/2019JA026909

Gelaro, R., W. McCarty, M. J. Suárez, et al., 2017: The modern-era retrospective analysis for research and applications, version 2 (MERRA-2). *Journal of climate*, **30**(14), 5419-5454, https://doi.org/10.1175/JCLI-D-16-0758.1

Harvey, V. L., and M. H. Hitchman, 1996: A climatology of the Aleutian High. *Journal*

of the atmospheric sciences, **53**(14), 2088-2102, https://doi.org/10.1175/1520-0469(1996)053<2088:ACOTAH>2.0.CO;2

Harvey, V. L., R. B. Pierce, T. D. Fairlie, et al., 2002: A climatology of stratospheric polar vortices and anticyclones. *Journal of Geophysical Research: Atmospheres*, **107**(D20), ACL-10, https://doi.org/10.1029/2001JD001471

Hu, Y., and K. K. Tung, 2002: Interannual and decadal variations of planetary wave activity, stratospheric cooling, and Northern Hemisphere annular mode. *Journal of Climate*, **15**(13), 1659-1673, https://doi.org/10.1175/1520-0442(2002)015<1659:IADVOP>2.0.CO;2

Haynes, P., 2005: Stratospheric dynamics. *Annu. Rev. Fluid Mech.*, **37**, 263-293, doi: 10.1146/annurev.fluid.37.061903.175710

Hu, Y., and Q. Fu, 2009: Stratospheric warming in Southern Hemisphere high latitudes since 1979. *Atmospheric Chemistry and Physics*, **9**(13), 4329-4340. https://doi.org/10.5194/acp-9-4329-2009

Hu, Y., Y. Xia, M. Gao, and D. Lu, 2009: Stratospheric Temperature Changes and Ozone Recovery in the 21st Century, *J. Meteor. Res*., **23**(3), 263-275.

Hu, D., W. Tian, F. Xie et al., 2015: Impacts of stratospheric ozone depletion and recovery on wave propagation in the boreal winter stratosphere. *Journal of Geophysical Research: Atmospheres*, **120**(16), 8299-8317, https://doi.org/10.1002/2014JD022855

Hu, D., Y. Guo, and Z. Guan, 2019: Recent weakening in the stratospheric planetary wave intensity in early winter. *Geophysical Research Letters*, **46**, 3953–3962,

https://doi.org/10.1029/2019GL082113

He, Y., X. Zhu, Z. Sheng, et al., 2022: Observations of Inertia Gravity Waves in the Western Pacific and Their Characteristic in the 2015/2016 Quasi - biennial Oscillation Disruption. *Journal of Geophysical Research: Atmospheres*, **127**, e2022JD037208, https://doi.org/10.1029/2021JD034719

Ivy, D. J., S. Solomon, and H. E. Rieder, 2016: Radiative and dynamical influences on polar stratospheric temperature trends. *Journal of Climate*, **29**(13), 4927-4938. DOI: https://doi.org/10.1175/JCLI-D-15-0503.1

Kodera, K., and Y. Kuroda, 2002: Dynamical response to the solar cycle. *Journal of Geophysical Research: Atmospheres*, **107**(D24), ACL-5, https://doi.org/10.1029/2002JD002224

Keckhut, P., C. Claud, B. Funatsu, et al., 2019: Temperature trends observed in the middle atmosphere and future directions. *Infrasound Monitoring for Atmospheric Studies: Challenges in Middle Atmosphere Dynamics and Societal Benefits*, 805-823, https://doi.org/10.1007/978-3-319-75140-5_26

Lin, P., Q. Fu, S. Solomon, et al., 2009: Temperature trend patterns in Southern Hemisphere high latitudes: Novel indicators of stratospheric change. *Journal of Climate*, **22**(23), 6325-6341, https://doi.org/10.1175/2009JCLI2971.1

Long, C. S., M. Fujiwara, S. Davis, et al., 2017: Climatology and interannual variability of dynamic variables in multiple reanalysis evaluated by the SPARC Reanalysis Intercomparison Project (S-RIP), *Atmos. Chem. Phys.*, **17**, 14593–14629, https://doi.org/10.5194/acp-17-14593-2017

Liu, H. L., M. Rempel, G. Danabasuglu, et al., 2023, Climate responses under an extreme quiet sun scenario. *Journal of Geophysical Research: Atmospheres,* e2022JD037626. https://doi.org/10.1029/2022JD037626

Matsuno, T., 1970: Vertical propagation of stationary planetary waves in the winter Northern Hemisphere. *Journal of Atmospheric Sciences*, **27**(6), 871-883. https://doi.org/10.1175/1520-0469(1970)027<0871:VPOSPW>2.0.CO;2

Matsuno, T., 1971: A dynamical model of the stratospheric sudden warming. *Journal of Atmospheric Sciences*, **28**(8), 1479-1494. https://doi.org/10.1175/1520-0469(1971)028<1479:ADMOTS>2.0.CO;2

Maycock, A. C., M. M. Joshi, K. P. Shine, et al., 2014: The potential impact of changes in lower stratospheric water vapour on stratospheric temperatures over the past 30 years. *Quarterly Journal of the Royal Meteorological Society*, **140**(684), 2176–2185, https://doi.org/10.1002/qj.2287

Maycock, A. C., W. J. Randel, A. K. Steiner, et al., 2018: Revisiting the mystery of recent stratospheric temperature trends. *Geophysical Research Letters*, **45**(18), 9919-9933, https://doi.org/10.1029/2018GL078035

McLandress, C., T. G. Shepherd, A. I. Jonsson, et al., 2015: A method for merging nadir-sounding climate records, with an application to the global-mean stratospheric temperature data sets from SSU and AMSU. *Atmospheric Chemistry and Physics*, **15**, 9271-9284, https://doi.org/10.5194/acp-15-9271-2015

Plumb, R. A., 1985: On the three-dimensional propagation of stationary waves. *Journal of the Atmospheric Sciences*, **42**(3), 217-229, https://doi.org/10.1175/1520-

0469(1985)042<0217:OTTDPO>2.0.CO;2

Ramaswamy, V., M. L. Chanin, J. Angell, et al., 2001: Stratospheric temperature trends: Observations and model simulations. *Reviews of Geophysics*, **39**(1), 71-122, https://doi.org/10.1029/1999RG000065

Randel, W. J., K. P. Shine, J. Austin, et al., 2009: An update of observed stratospheric temperature trends. *Journal of Geophysical Research: Atmospheres*, **114**(D2), https://doi.org/10.1029/2008JD010421

Randel, W. J., A. K. Smith, F. Wu, et al., 2016: Stratospheric temperature trends over 1979–2015 derived from combined SSU, MLS, and SABER satellite observations. *Journal of Climate*, **29**(13), 4843-4859, https://doi.org/10.1175/JCLI-D-15-0629.1

Remsberg, E., G. Lingenfelser, V. L. Harvey, et al., 2003: On the verification of the quality of SABER temperature, geopotential height, and wind fields by comparison with Met Office assimilated analyses. *Journal of Geophysical Research: Atmospheres*, **108**(D20), 4628, https://doi.org/10.1029/2003JD003720

Remsberg, E. E., B. T. Marshall, M. Garcia-Comas, et al., 2008: Assessment of the quality of the Version 1.07 temperature-versus-pressure profiles of the middle atmosphere from TIMED/SABER. *Journal of Geophysical Research: Atmospheres*, **113**, D17101, https://doi.org/10.1029/2008JD010013

Remsberg, E., 2019: Observation and attribution of temperature trends near the stratopause from HALOE. *Journal of Geophysical Research: Atmospheres* 124.12, 6600-6611, doi: 10.1029/2019JD030455

Shine, K. P., M. S. Bourqui, P. D. F. Forster, et al., 2003: A comparison of

model-simulated trends in stratospheric temperatures. *Quarterly Journal of the Royal Meteorological Society*, **129**(590), 1565-1588, https://doi.org/10.1256/qj.02.186

Smith, K. L., C. G. Fletcher, and P. J. Kushner, 2010: The role of linear interference in the annular mode response to extratropical surface forcing. *Journal of Climate*, **23**(22), 6036-6050. https://doi.org/10.1175/2010JCLI3606.1

Seidel, D. J., N. P. Gillett, J. R. Lanzante, et al., 2011: Stratospheric temperature trends: Our evolving understanding. *Wiley Interdisciplinary Reviews: Climate Change*, **2**(4), 592-616, https://doi.org/10.1002/wcc.125

Seidel, D. J., J. Li, C. Mears, et al., 2016: Stratospheric temperature changes during the satellite era. *Journal of Geophysical Research: Atmospheres*, **121**(2), 664-681, https://doi.org/10.1002/2015JD024039

Rao, J., R. Ren, and Y. Yang, 2015: Parallel comparison of the northern winter stratospheric circulation in reanalysis and in CMIP5 models. *Advances in Atmospheric Sciences*, **32**, 952-966. https://doi.org/10.1007/s00376-014-4192-2

Steiner, A. K., F. Ladstädter, W. J. Randel, et al., 2020: Observed temperature changes in the troposphere and stratosphere from 1979 to 2018. *Journal of Climate*, **33**(19), 8165-8194. DOI: https://doi.org/10.1175/JCLI-D-19-0998.1

Thompson, D. W., and S. Solomon, 2009: Understanding recent stratospheric climate change. *Journal of Climate*, **22**(8), 1934-1943, https://doi.org/10.1175/2008JCLI2482.1

Thompson, D. W., D. J. Seidel, W. J. Randel, et al., 2012: The mystery of recent stratospheric temperature trends. *Nature*, **491**(7426), 692-697,

https://doi.org/10.1038/nature11579

Wang, L., C.-Z. Zou, and H. Qian, 2012: Construction of stratospheric temperature data records from stratospheric sounding units. *J. Climate*, **25**, 2931–2946, doi:10.1175/JCLI-D-11-00350.1.

WMO, 2018: *WMO statement on the state of the global climate in 2017*. World Meteorological Organisation, Geneva.

Xia, Y., Xu, W., Hu, Y. et al., 2020: Southern-Hemisphere high-latitude stratospheric warming revisit. Clim Dyn 54, 1671–1682. https://doi.org/10.1007/s00382-019-05083-7

Yamashita, C., H. L. Liu, and X. Chu, 2010: Gravity wave variations during the 2009 stratospheric sudden warming as revealed by ECMWF‐T799 and observations. *Geophysical Research Letters*, **37**(22), https://doi.org/10.1029/2010GL045437

Zou, C. Z., M. Gao, and M. D. Goldberg, 2009: Error structure and atmospheric temperature trends in observations from the Microwave Sounding Unit. *Journal of Climate*, **22**(7), 1661-1681, https://doi.org/10.1175/2008JCLI2233.1

Zou, C. Z., and H. Qian, 2016: Stratospheric temperature climate data record from merged SSU and AMSU-A observations. *Journal of Atmospheric and Oceanic Technology*, **33**(9), 1967-1984, https://doi.org/10.1175/JTECH-D-16-0018.1

Zhou, L., Y. Xia, and C. Zhao, 2022: Influence of Stratospheric Ozone Changes on Stratospheric Temperature Trends in Recent Decades, *Remote Sensing*, **14**(21), 5364. https://doi.org/10.3390/rs14215364

Responses to reviewers

Zonally Asymmetric Temperature Trends near the Northern Middle and High Latitude Stratopause during Winter

Tao Wang[1], Wenshou Tian[1]*, Ruhua Zhang[2], Jiali Luo[1], Wuhu Feng[3]

[1] *College of Atmospheric Sciences, Lanzhou University, Lanzhou, Gansu, China*

[2] *Department of Atmospheric and Oceanic Sciences and Institute of Atmospheric Sciences, Fudan University, Shanghai, China*

[3] *NCAS, School of Earth and Environment, University of Leeds, Leeds, UK.*

Corresponding author : Wenshou Tian (wstian@lzu.edu.cn)

Manuscript number of the previous submission：ACTA-E-2023-0015.R1

April 2023

We sincerely appreciate the three reviewers for their valuable comments and suggestions to improve the quality of our manuscript. The following is the detailed response to the comment of Reviewer 3.

Response to the Comment of Reviewer 3

Comments to the Author

The authors have basically responded well to my previous comments, and the revised manuscript needs minor modifications.

About the previous comment (3)

The zonally symmetric pattern generally means the latitudinal variation at different latitudes. The longitudinal variation at some latitude as you said, is misleading.

Response: We thank the reviewer's careful reading and helpful comment. We double check the original manuscript and find the misleading is induced that we intended to say "the zonally asymmetric pattern", but due to our oversight, it came out as "zonally symmetric pattern". The whole paper is about the zonally asymmetric temperature trend pattern. Therefore, "zonally symmetric" in L483-484 and L573-580 in the original manuscript (or L422-429 in the last revised manuscript) are mistakes. They should be "zonally asymmetric" and are now corrected (please see L423-430 in the revision). Also, our previous response to the major comment (3) should be "But the zonally asymmetric pattern means the longitudinal variation at certain latitudes, not the zonal mean variation.", which may make sense and not be misleading.

Zonally Asymmetric Temperature Trends near the Northern Middle and High Latitude Stratopause during Winter

Tao Wang[1], Wenshou Tian[1*], Ruhua Zhang[2], Jiali Luo[1], Wuhu Feng[3]

[1] *College of Atmospheric Sciences, Lanzhou University, Lanzhou* 730000*, China*

2 Department of Atmospheric and Oceanic Sciences and Institute of Atmospheric Sciences, Fudan University, Shanghai, China

[3] *NCAS, School of Earth and Environment, University of Leeds, Leeds, UK.*

(Submitted January 29, 2023)

This work is partly supported by the National Natural Science Foundation of China (42130601, 42142038).

*Corresponding author: Wenshou Tian (wstian@lzu.edu.cn). Tel: 18509486025

Abstract

The temperature trend near the stratopause is rarely evaluated owing to the limited long-term observations of global temperature. In this study, the spatial patterns of the temperature trends near the stratopause are investigated using satellite and reanalysis datasets. Our analysis reveals a zonally asymmetric temperature trend pattern near the northern mid-to-high latitude stratopause during January, and this ~~zonally asymmetric temperature trend~~ pattern underwent an evident transition around the 2000s. From 1980 to 2003, there was a cooling trend in the western hemisphere and a warming trend in the eastern hemisphere. In contrast, a reversed zonally asymmetric temperature trend pattern existed in the east-west direction from 2003 to 2020. Although the warming trends are statistically insignificant, they contrasted with the overall cooling trend in the upper stratosphere due to ozone depletion and an increase in well-mixed greenhouse gases in recent decades. The zonally asymmetric temperature trends were induced by the transition in the intensity of quasi-stationary planetary wavenumber 1 (wave 1) near the stratopause. The increasing (decreasing) trend of the intensity of wave 1 enhanced (reduced) its meridional temperature advection near the stratopause before (after) the 2000s, consequently, a zonally asymmetric temperature trend pattern exists in the east-west direction near the stratopause. The transition in the intensity of the stratospheric wave 1 around the 2000s is most likely caused by the transition in the intensity of wave 1 activity in the troposphere.

Key words: Stratospheric temperature trend, zonally asymmetric temperature pattern, quasi-stationary planetary wavenumber 1

1. Introduction

The stratospheric temperature is a crucial climate marker that is affected by both thermal-dynamic and chemical processes. In response to ozone depletion and increasing well-mixed greenhouse gases (GHGs), the stratospheric temperature has experienced a significant cooling trend over the past several decades, which has been noted by a wide variety of observations and reproduced by multiple climate models (e.g., Golitsyn et al., 1996; Ramaswamy et al., 2001; Wang et al., 2012; Thompson et al., 2009, 2012; Randel et al., 2009, 2017; Rao et al., 2015; Garcia et al., 2019; Remsberg, 2019; Steiner et al., 2020). Notably, recently updated and extended satellite data has provided relatively reliable zonal mean temperature observations throughout the stratosphere and revealed that the zonal mean temperature trends decreased with altitude from the lower stratosphere to the upper stratosphere from 1979 to 2015 (McLandress et al., 2015; Randel et al., 2016; Zou and Qian, 2016). However, the long-term trends in stratospheric temperature still have uncertainties in both their magnitudes and spatial variations (e.g., Shine et al., 2003; Fu et al., 2010; Seidel et al., 2011; Funatsu et al., 2016; Maycock et al., 2018). These uncertainties are partly due to discrepancies in different observations (e.g., Zou et al., 2009; Thompson et al., 2012; Keckhut et al., 2019; Seidel et al., 2016) and are partly relate to the challenges involved in clarifying the factors that contribute to stratospheric temperature trends (e.g., Hu and Fu, 2009; Hu et al., 2009; Ivy et al., 2016; Xia et al., 2020; Zhou et al., 2022).

Various factors may influence temperature trends in the stratosphere. Although well-mixed GHGs are still increasing, a weak recovery signal has appeared in

stratospheric ozone in the last two decades (e.g., Hu et al., 2015; Chipperfield et al., 2017). Consequently, future trends in stratospheric temperatures (Arblaster et al., 2014; WMO, 2018) will mainly result from the opposing effects of increasing CO_2 (colder stratosphere) and increasing ozone (the warmer stratosphere). Moreover, the increasing stratospheric water vapor and volcanic aerosols have potentially impacted the temperature trends in the tropical lower stratosphere in recent decades (e.g., Maycock et al., 2014). Apart from the radiative contributions of chemical constituents, dynamic processes also have a large impact on stratospheric temperature trends, particularly at middle and high latitudes. It is known that temperatures in the stratosphere at middle and high latitudes are dominated by both ~~by~~ the radiative balance and dynamic heating originating from tropospheric wave forcing (Andrews et al., 1987; Haynes, 2005; He et al., 2022). Given that GHGs trends are monotonically increasing, the temperature trends in the stratosphere at middle and high latitudes are strongly modulated by changes in planetary wave forcing in the stratosphere (Hu and Tung, 2002; Fu et al., 2019). As a result, the large interannual and decadal variations in dynamical forcing may lead to large uncertainties in stratospheric temperature trends (e.g., Matsuno, 1971; Yamashita et al., 2010; Long et al., 2017).

On the other hand, previous studies have mainly focused on trends in global or zonal mean temperatures in the stratosphere, but the longitudinal variations in the temperature trend in the stratosphere have rarely been evaluated. In particular, the spatial variations in the temperature trend near the stratopause are still poorly understood due to the shortage of long-term global observations there. It is well known

that the polar night jet is persistent in the Northern Hemisphere (NH) winter, indicating strong baroclinicity there (France and Harvey, 2013; Harvey et al., 2002). Harvey and Hitchman (1996) noted that the maximum longitudinal differences between the Aleutian High and the polar vortex were located near the stratopause. In addition, previous studies have reported the shift in the tropospheric and stratospheric climate around the 2000s (e.g., Chen and Tung, 2014; Hu et al., 2019~~), if~~). However, whether the climate shift occurs near the stratopause is still unclear. Therefore, it is of interest to investigate ~~recent variations~~the changes in the temperature near the stratopause in recent decades.

In this study, we employ the Modern-Era Retrospective Analysis for Research and Applications, version 2 (MERRA-2) reanalysis datasets from 1980 to 2020 and the TIMED/SABER satellite temperature data from 2003 to 2020 to investigate spatial variations in the temperature trend near the stratopause during the ~~NH~~northern winter as well as the possible factors responsible for the temperature trends near the stratopause. The organization of our paper is as follows. Section 2 describes the data and method we used. In Section 3, we exhibit and compare the temperature trends near the stratopause ~~in NH~~during the northern winter derived from TIMED/SABER observations and the MERRA-2 reanalysis dataset. In Section 4, we investigate possible factors responsible for the temperature trends. The conclusions and discussions are summarized in Section 5.

2. Data and Methods

2.1 Data

SABER is an infrared limb sounder launched on the TIMED satellite, which provides reliable global temperature data above the troposphere. Its latitudinal coverage ranges from a north-looking mode (53°S–83°N) to a south-looking mode (53°N–83°S) approximately every 60 days. The SABER temperature profiles have been retrieved from infrared emissions of CO_2 from approximately 16 km to 105 km altitude with an effective vertical resolution of 2 km. TIMED/SABER temperature has been evaluated by Remsberg et al. (2003, 2008). In this study, we use the TIMED/SABER (version 2.0) temperature dataset from 2003 to 2020 and bin the data into 2° × 4° (longitude by latitude) monthly mean maps.

–MERRA-2 is produced by the National Aeronautics and Space Administration (NASA) Global Modeling and Assimilation Office (GMAO). The temperature data from the Microwave Limb Sounder (MLS) are assimilated in MERRA-2 above 5 hPa, providing more accurate temperature data for the upper stratosphere than MERRA (Gelaro et al. (2017). The zonal mean temperature comparisons between observations and reanalysis datasets, including MERRA-2, were investigated by Long et al. (2017). ~~Here, the~~The MERRA-2 instM_3d_asm_Np monthly mean datasets (Version 5.12.4) are used ~~over~~during the period from 1980 to 2020, with a horizontal resolution of 0.5° × 0.625° (latitude × longitude) and 42 vertical levels up to a height of 0.1 hPa.

2.2 Method

In this study, the Eliassen-Palm (EP) flux (Andrews et al., 1987) and the Plumb flux (Plumb, 1985) are applied to measure the strength and propagation of wave activities in two dimensions and three dimensions, respectively. The meridional ($F^{(\varphi)}$)

and vertical ($F^{(z)}$) components of the EP flux and its divergence ($\nabla \cdot \boldsymbol{F}$) are defined as follows:

$$F^{(\varphi)} = \rho_0 a\cos\varphi\left(\overline{u_z}\frac{\overline{v'\theta'}}{\overline{\theta_z}} - \overline{u'v'}\right) \quad (1)$$

$$F^{(z)} = \left(f - \frac{(\overline{u}\cos\varphi)_\varphi}{a\cos\varphi}\right)\frac{\overline{v'\theta'}}{\overline{\theta_z}} - \overline{u'w'} \quad (2)$$

$$\nabla \cdot \boldsymbol{F} = \frac{\partial F^{(\varphi)}}{\partial \varphi} + \frac{\partial F^{(z)}}{\partial z} \quad (3)$$

where φ is latitude, z is height, ρ is air density, a is the Earth's radius, f is the Coriolis parameter, θ is potential temperature, u is zonal wind, v is meridional wind, and w is vertical wind. The overbars and primes denote the zonal mean and the departure from the zonal mean, respectively. The subscript 0 is for the background variables. The subscript z is for the partial derivative for the variables in the vertical direction.

The longitude ($F^{(\lambda)}$), latitude ($F^{(\varphi)}$), and vertical ($F^{(z)}$) components of the Plumb flux and its divergence ($\nabla \cdot \boldsymbol{F}$) are defined as follows:

$$F^{(\lambda)} = \rho_0\cos\varphi\ \left(\frac{1}{2a^2\cos^2\varphi}\left[\left(\frac{\partial\psi'}{\partial\lambda}\right)^2 - \psi'\frac{\partial^2\psi'}{\partial\lambda^2}\right]\right) \quad (4)$$

$$F^{(\varphi)} = \rho_0\cos\varphi\ \left(\frac{1}{2a^2\cos^2\varphi}\left[\frac{\partial\psi'}{\partial\lambda}\frac{\partial\psi'}{\partial\varphi} - \psi'\frac{\partial^2\psi'}{\partial\lambda\partial\varphi}\right]\right) \quad (5)$$

$$F^{(z)} = \rho_0\cos\varphi\ \left(\frac{2\Omega^2\sin^2\varphi}{N^2 a\cos\varphi}\left[\frac{\partial\psi'}{\partial\lambda}\frac{\partial\psi'}{\partial z} - \psi'\frac{\partial^2\psi'}{\partial\lambda\partial z}\right]\right) \quad (6)$$

$$\nabla \cdot \boldsymbol{F} = \frac{\partial F^{(\lambda)}}{\partial \lambda} + \frac{\partial F^{(\varphi)}}{\partial \varphi} + \frac{\partial F^{(z)}}{\partial z} \quad (7)$$

where λ is longitude, Ω is the Earth's angular velocity, N is the Brunt–Väisälä frequency, $\psi = \Phi/2\Omega\sin\varphi$, and Φ is potential height.

3. Temperature Trends Near the Stratopause ~~in~~

~~NH~~during the Northern Winter

Figs. 1a and 1c present the spatial patterns of the 3 hPa temperature trends over the NH during January from 1980-2003 and from 2003-2020 derived from MERRA-2 reanalysis data, respectively. A noticeable feature is that there is a zonally asymmetric pattern in temperature trends at mid-high latitudes shown in Fig. 1a, with a cooling trend in the western hemisphere and a warming trend in the eastern hemisphere. In contrast, a reversal temperature trend in the east-west direction can be noted in Fig. 1c, with a warming (cooling) trend in the western (eastern) hemisphere. Note that the results here are not sensitive to slight changes in the starting/ending year of the time series. Thompson et al. (2012) indicated that due to ozone depletion and increasing well-mixed GHGs in recent decades, the stratospheric cooling in the upper stratosphere is more robust than that in the lower-middle stratosphere. Hence, although these warming trends in Figs. 1a and 1c are statistically insignificant at the 95% confidence level, they contrast with the overall cooling trend in the upper stratosphere. To understand the unusual warming near the stratopause, we separate the temperature into two components, i.e., zonal mean and deviations from the zonal mean (hereafter zonal temperature deviations). The zonal mean temperature denotes the background field, which is dominated by chemical and radiative balances. The temperature deviations denote the disturbed field, which is largely controlled by adiabatic/diabatic thermodynamic processes.

Figs. 1b and 1d show the spatial patterns of trends in zonal temperature deviations at 3 hPa over the NH during January from 1998 to 2003 and from 2003 to 2020 derived from MERRA-2 reanalysis data, respectively. The trends in zonal temperature deviations also present zonally asymmetric patterns at mid-high latitudes, with a statistically significant cooling (warming) trend in the western (eastern) hemisphere in Fig. 1b, and a reversal temperature trend in the east-west direction in Fig. 1d. The warming (cooling) trends in the zonal temperature deviations are stronger (weaker) compared to those in the original temperature. The green counters superimposed on Figs. 1b and 1d are the climatology of the zonal temperature deviations, which are likewise zonally asymmetric at mid-high latitudes, with negative (positive) anomalies in the western (eastern) hemisphere. The climatology of the zonal temperature deviations is generally in phase (out of phase) with the trends of the zonal temperature deviations in Fig. 1b (1d), suggesting that the zonal asymmetry of temperature variations was strengthened (weakened) before (after) the 2000s, and there was a transition in the zonally asymmetric temperature trend pattern around the 2000s.

The latitudinal variations in the 3 hPa zonal mean temperature trends over the NH during January from 1980 to 2003 and from 2003 to 2020 derived from MERRA-2 reanalysis data are shown in Fig. 1g, respectively. The morphology of zonal mean temperature trend before the 2000s is similar to that after the 2000s. The zonal mean temperature trend is close to zero at lower latitudes but decreases with increasing latitudes at mid-high latitudes. Overall, the zonal mean temperature trend before/after the 2000s is cooling in the NH, which is consistent with the increase in well-mixed GHGs in recent decades. The results shown in Fig. 1 as derived from MERRA-2 reanalysis data suggest that the zonal asymmetry of the temperature trends near the stratopause is the product of changes in disturbed fields.

To further verify the trends exhibited in Fig. 1 derived from MERRA-2 reanalysis data, TIMED/SABER satellite temperature observations (from 2003-2020) are analyzed. Figs. e, f, and g (blue line) are the same as Figs. c, d, and g (red line), respectively, but the data is derived from TIMED/SABER observations. It is seen that the zonally asymmetric temperature trend pattern is also apparent in TIMED/SABER observations, and the corresponding results derived from MERRA-2 reanalysis data agree well with those derived from TIMED/SABER observations in both morphology and magnitude. Since the temperature trends near the stratopause in MERRA-2 reanalysis data are in good agreement with those from the TIMED/SABER temperature observations, the MERRA-2 dataset is utilized to investigate the possible factors responsible for the zonally asymmetric variations in the temperature. Note that the spatial pattern of 3 hPa temperature shows an almost uniform cooling trend over the NH during January from 1980 to 2020 derived from MERRA-2 reanalysis data (not shown).

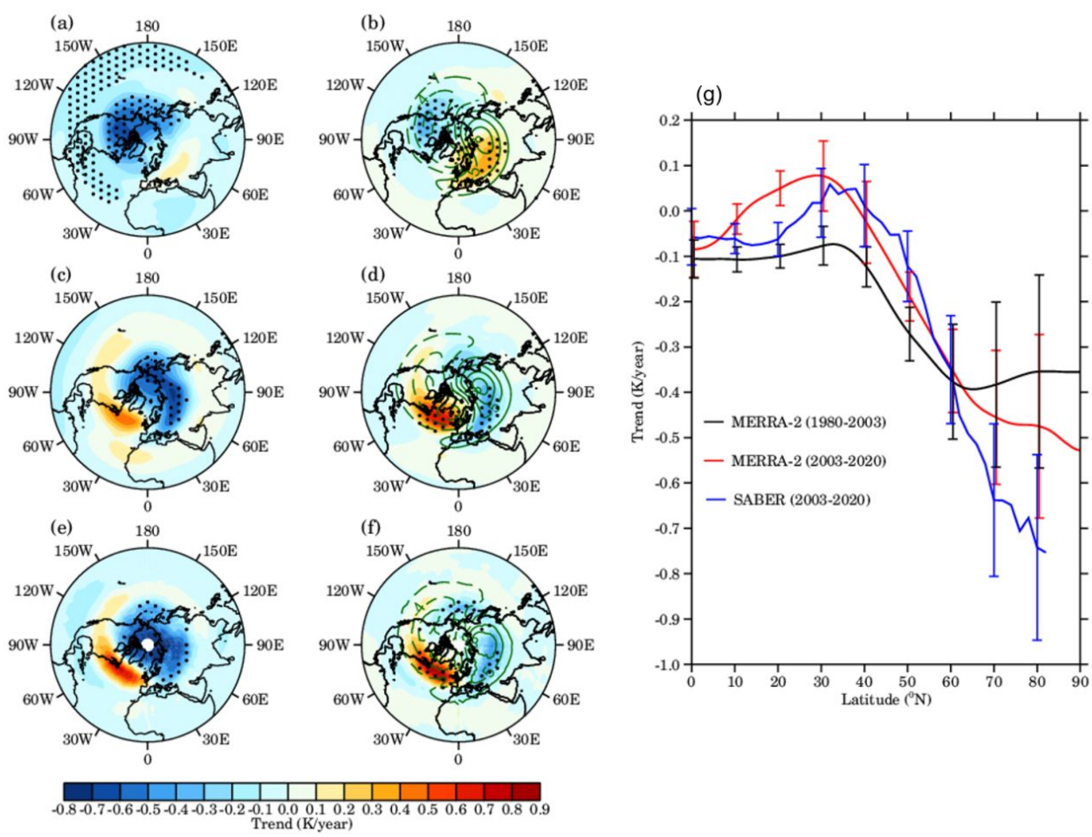

Fig. 1. Spatial pattern of trends in (a) temperature and (b) zonal temperature deviations over the NH at 3 hPa during January from 1980 to 2003 derived from MERRA-2 reanalysis data. (c) and (d) are the same as (a) and (b), respectively, but the time period is from 2003 to 2020. (e) and (f) are the same as (c) and (d), respectively, but the data is derived from TIMED/SABER observations. The values over the stippled areas are statistically significant at the 95% confidence level according to Student's t test. The green contour lines denote the climatology of the zonal temperature deviations (the contour interval is 3 K, solid and dashed lines indicate positive and negative values, respectively). (g) Latitude variations in the zonal mean temperature trends over the NH at 3 hPa during January from 1980 to 2003 derived from MERRA-2 reanalysis dataset (black line), from 2003 to 2020 derived from MERRA-2 reanalysis dataset (red line), and from 2003 to 2020 derived from TIMED/SABER observations (blue line). Error

bars show the 2σ statistical uncertainty.

Fig. 2 presents the time series of the zonal temperature deviations averaged over the climatological high-temperature lobe (hereafter East) (50°N-70°N, 30°E-180°E) (solid lines) and the climatological low-temperature lobe (hereafter West) (50°N-70°N, 0-150°W) (dashed lines) at 3 hPa during January from 1980 to 2020 derived from MERRA-2 reanalysis data (black lines) and from 2003 to 2020 derived from TIME/SABER observations (blue lines), respectively. The straight lines represent the linear fits of the zonal temperature deviations before and after 2003, respectively. The time series of the zonal temperature deviations derived from MERRA-2 agree well with those derived from the TIMED/SABER observations in both magnitudes and variations. The East underwent a statistically significant increasing trend (0.1 K/year) from 1980 to 2003 and a statistically significant decreasing trend (-0.17 K/year) from 2003 to 2020. The West has similar magnitudes but opposite signs in both interannual variations and long-term trends compared to the East, indicating a close negative correlation in the zonal temperature deviations between the two lobes. The correlation coefficients between the East and West are -0.89 (-0.90) derived from the MERRA-2 reanalysis data (TIMED/SABER observations). Note that the results here are not sensitive to slight changes in the latitude/longitude bounds used for averaging the data.

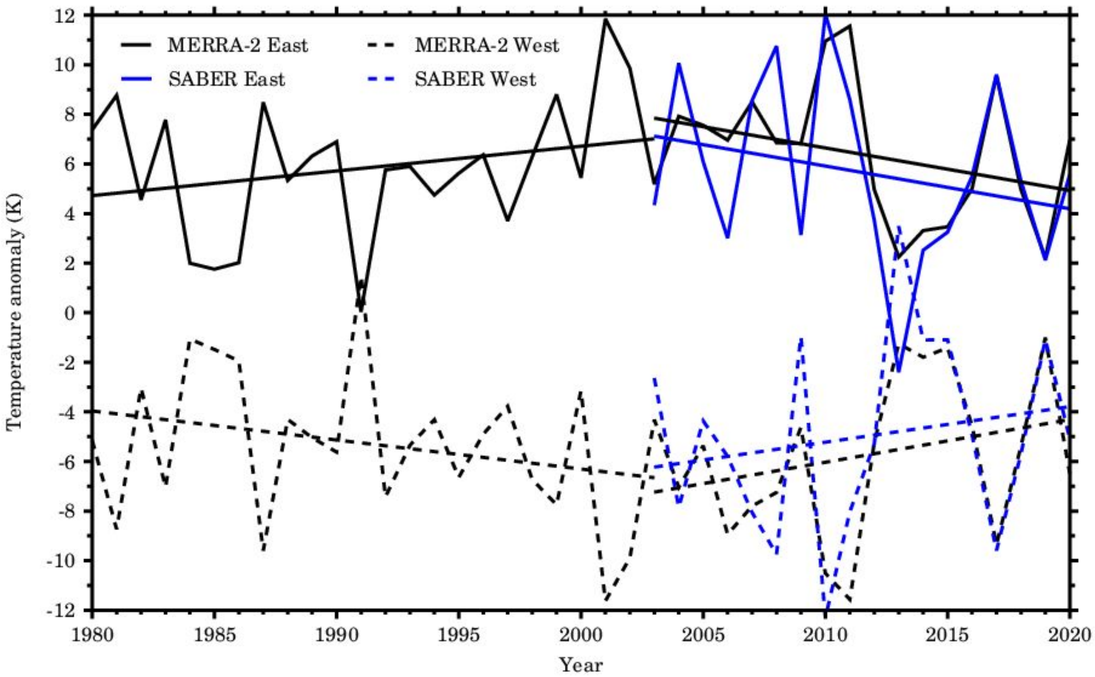

Fig. 2. Time series of the zonal temperature deviations averaged over the climatological high-temperature lobe (hereafter East) (50°N-70°N, 30°E-180°E) (solid lines) and the climatological low-temperature lobe (hereafter West) (50°N-70°N, 0-150°W) (dashed lines) at 3 hPa during January from 1980 to 2020 derived from the MERRA-2 reanalysis data (black lines) and from 2003 to 2020 TIME/SABER observations (blue lines), respectively. The straight lines represent the linear fits of the zonal temperature deviations before and after 2003, respectively.

To depict the zonally asymmetric temperature trend variations with heights, Fig. 3 shows the longitude-height cross sections of the trends in zonal temperature deviation at 70°N during January (a) from 1980 to 2003 derived from MERRA-2 reanalysis data ~~(a),~~, (b) from 2003 to 2020 derived from MERRA-2 reanalysis data ~~(b),~~, and (c) from 2003 to 2020 derived from TIMED/SABER observations ~~(c).~~. The black contours superimposed on Fig. 3 denote the climatology of the zonal temperature deviations. The climatology of the zonal temperature deviations in the upper stratosphere and lower mesosphere (hereinafter USLM) also present a zonally asymmetric pattern, with the climatological high-temperature (low-temperature) lobe mainly located in the eastern (western) hemisphere. The climatology of the zonal temperature deviations tilts westward with heights, exhibiting a pattern analogous to that of the quasi-stationary planetary wavenumber 1 (wave 1).

As shown in Fig. 3a, the trend in the zonal temperature deviation is generally in phase with the climatology of the zonal temperature deviation in the USLM, with a statistically significant warming (cooling) trend in the eastern (western) hemisphere near the stratopause before the 2000s. In contrast, Fig. 3b shows the trend in the zonal temperature deviation is generally out of phase with the climatology of the zonal temperature deviation in the USLM, with a statistically significant cooling (warming) trend mainly located in the eastern (western) hemisphere near the stratopause after the 2000s. The longitude-height cross section of the zonal temperature deviation derived from MERRA-2 reanalysis data (Fig. 3b) is comparable to that derived from TIMED/SABER observations (Fig. 3c). The results in Fig. 3 further support that the zonally asymmetric temperature trend pattern undergoes a transition in the east-west direction around the 2000s and is most pronounced near the stratopause.

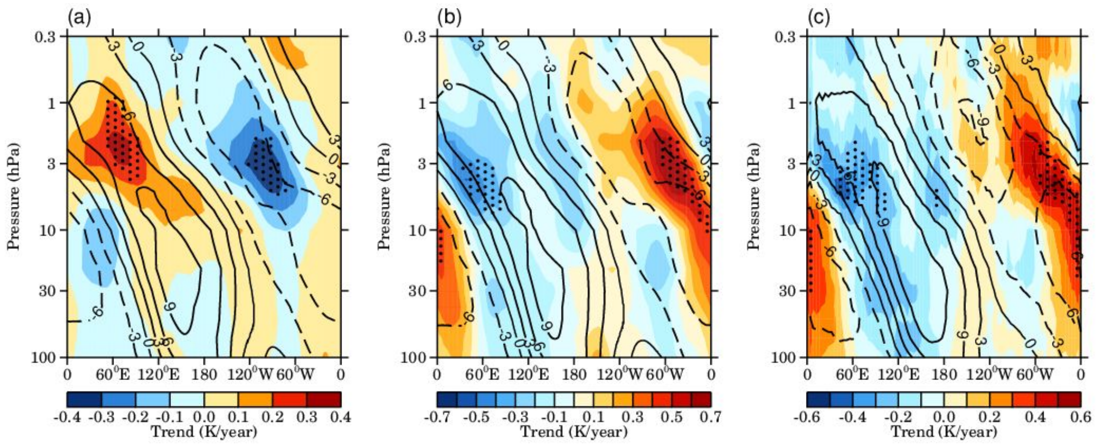

Fig. 3. Longitude-height cross sections of the trends (color shading) and climatology (black contours, the contour interval is 3 K, solid and dashed lines indicate positive and negative values, respectively) of zonal temperature deviations at 70°N during January (a) from 1980 to 2003 derived from MERRA-2 reanalysis dataset, (b) from 2003 to 2020 derived from MERRA-2 reanalysis dataset, and (c) from 2003 to 2020 derived from TIMED/SABER observations. The values over the stippled areas are statistically significant at the 95% confidence level according to Student's t test.

4. Factors Responsible for the Temperature Trends

The previous section mentioned that the zonally asymmetric temperature trends near the NH stratopause result from changes in the zonal temperature deviations and may be controlled by thermodynamic factors. France et al. (2012) reported that the advection and dissipation of quasi-stationary planetary waves could largely influence the spatial structure of temperatures at mid-high latitudes in the upper stratosphere. Therefore, the contributions of wave activities to the zonally asymmetric temperature trends are first examined here. Figs. 4a and 4d shows the latitude-height distributions of the trends in the EP flux (green vectors) and its divergence (color shading) during January from 1980 to 2003 and from 2003 to 2020 derived from MERRA-2 reanalysis

datasets, respectively. The signs of trends in EP flux are upward (downward) from the troposphere to the lower mesosphere at mid-high latitudes, indicating enhanced (weakened) wave activities throughout the troposphere and stratosphere before (after) the 2000s. In particular, the magnitudes of EP flux trends are robust in the mid-high latitude USLM, where the zonally asymmetric temperature trends exist. The negative (positive) trend in EP flux divergence is robust and statistically significant near the mid-high latitudes stratopause, supporting the enhanced (weakened) wave activities are most pronounced near the mid-high latitudes stratopause before (after) the 2000s. The trends of EP flux and its divergence in Fig. 4a are generally opposite to those in Fig. 4d, indicating the intensity of wave activities also underwent a transition around the 2000s from the troposphere to the lower mesosphere at mid-high latitudes.

According to Fig. 3, the climatology and trends of the zonal temperature deviations in the mid-high latitude USLM display a wave 1 pattern, suggesting that wave 1 activities may play a key role in modulating zonal temperature deviations. Therefore, we separate total waves into wave 1 and residual waves. Figs. 4b and 4e are the same as Figs. 4a and 4d, but for the EP flux and its divergence associated with wave 1, respectively. Figs. 4c and 4f are the same as Figs. 4a and 4d, but for the EP flux and its divergence associated with residual waves, respectively. The morphology and magnitude shown in Fig. 4b (4e) are much similar to those in Fig. 4a (Fig. 4d), confirming that the intensity of wave 1 are enhanced (weakened) before (after) the 2000s, and the changes in wave activities are dominated by changes in wave 1 activities. Besides, Fig. 4c depicts that the EP flux and its divergence associated with residual

waves do not show statistically significant changes in the USLM from 1980 to 2003. Fig. 4f presents a statistically significant negative trend in EP flux divergence in the high latitude upper stratosphere, along with the upward sign of the EP flux trend, which indicates that the intensity of residual waves is enhanced in this region from 2003 to 2020 but is contrary to that of wave 1 (Fig. 4e). The combine effects of enhanced residual waves and weakened wave 1 result in slightly weakened total waves in this region (Fig. 4d).

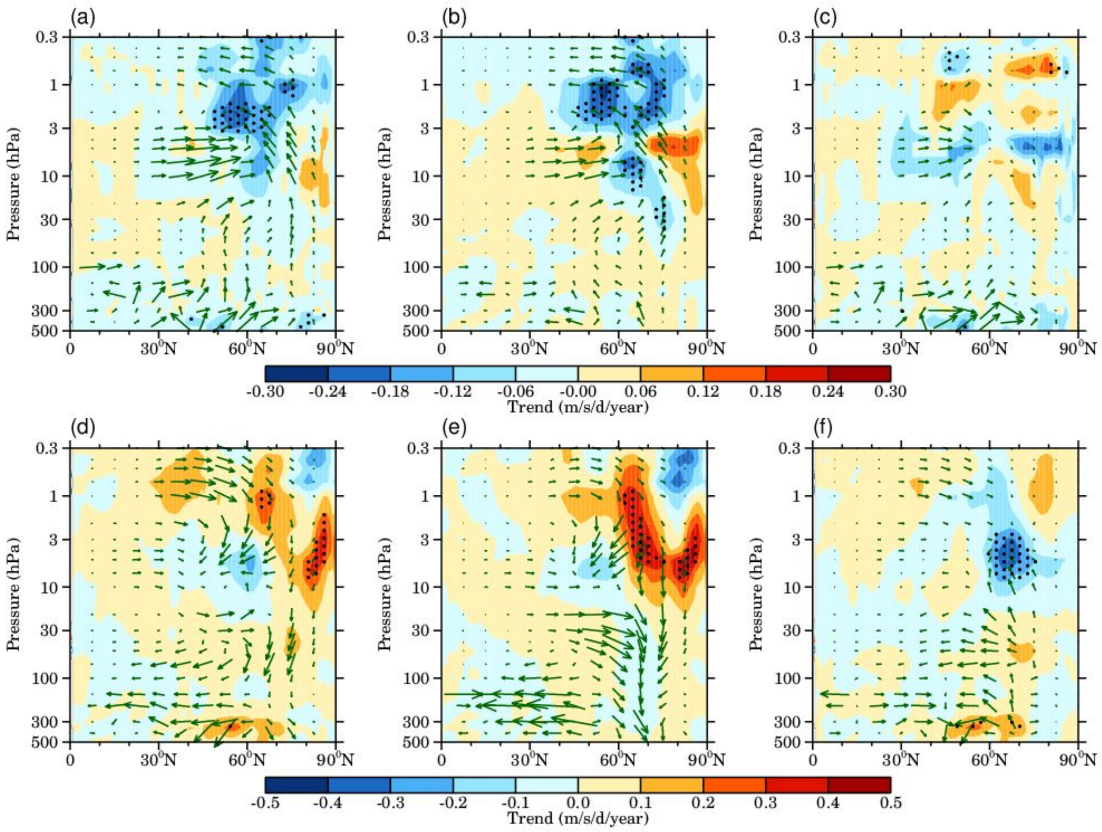

Fig. 4. (a) Latitude-height distribution of trends in Eliassen-Palm (EP) fluxes (green vectors, units in the horizontal and vertical components are 10^{-2} and 10^{-4} m^2/s^2/year, respectively) and the EP flux divergence (color shading) in January during the period from 1980 to 2003. (b) The same as (a), but for the EP flux and its divergence associated

with wave 1. (c) The same as (a), but for the EP flux and its divergence associated with residual waves. (d), (e), and (f) are the same as (a), (b), and (c), respectively, but the time period is from 2003 to 2020. The EP fluxes are multiplied by the square root of 1000/pressure (hPa). The trends over stippled areas are statistically significant at the 95% confidence level according to Student's t test. The results are derived from the MERRA-2 reanalysis dataset.

Since the changes in zonal mean wave 1 activities underwent a transition around the 2000s, which is coincident with the changes in the zonally asymmetric temperature trend patten, we further examine the zonal variations in wave 1 and the effects of wave 1 on the zonally asymmetric temperature variations. Figs. 5a and 5c present the longitude-height cross sections of the trends (color shading) and climatology (black contours) of temperature associated with wave 1 at 70°N during January from 1980 to 2003 and from 2003 to 2020 derived from the MERRA-2 reanalysis dataset, respectively. The temperature trends associated with wave 1 tilt westward with heights and are generally in phase (out of phase) with their climatology throughout the stratosphere, indicating enhanced (weakened) wave 1 activities before (after) the 2000s. In particular, the temperature trends associated with wave 1 are robust and statistically significant near the stratopause. The results in Fig. 5 are comparable to those in Fig. 3 in the USLM, indicating the changes in wave 1 are responsible for the changes in zonal temperature deviations. Moreover, Both Figs. 5a and 5c show statistically significant temperature trends associated with wave 1 in the troposphere, suggesting significant changes in the tropospheric wave 1 before and after the 2000s, respectively. The green

vectors superimposed on Figs. 5a and 5c are the trends of Plumb fluxes associated with wave 1. The signs of the trends of Plumb flux associated with wave 1 are upward (downward) from the troposphere and the lower mesosphere, which further supports enhanced (weakened) wave 1 activities from the troposphere and the lower mesosphere within the whole latitudinal band before (after) the 2000s.

Figs. 5b and 5d are the same as Figs. 5a and 5c, respectively, but for the meridional wind associated with wave 1. Likewise, the trend of the meridional wind associated with wave 1 is in phase (out of phase) with the climatology of the meridional wind associated with wave 1 from the troposphere to the lower mesosphere before (after) the 2000s. The strongest amplitude of the meridional wind associated with wave 1 is near the stratopause and dominates the meridional wind there (Andrews et al, 1987). The poleward (equatorward) meridional wind associated with wave 1 induces warm (cold) meridional temperature advection in the eastern (western) hemispheres near the stratopause, resulting in the climatological high-temperature (low-temperature) mainly located in the eastern (western) hemispheres. Since the intensity of wave 1 is strengthened (weakened) before (after) the 2000s, it enhances (reduces) the meridional temperature advection near the stratopause; consequently, the zonally asymmetric trends in zonal temperature deviations are in phase (out of phase) with their climatology near the stratopause. Gabriel et al. (2007, 2011a) also noted that the wave 1 structure of temperature near the stratopause is controlled by zonally asymmetric transport by geostrophically balanced winds.

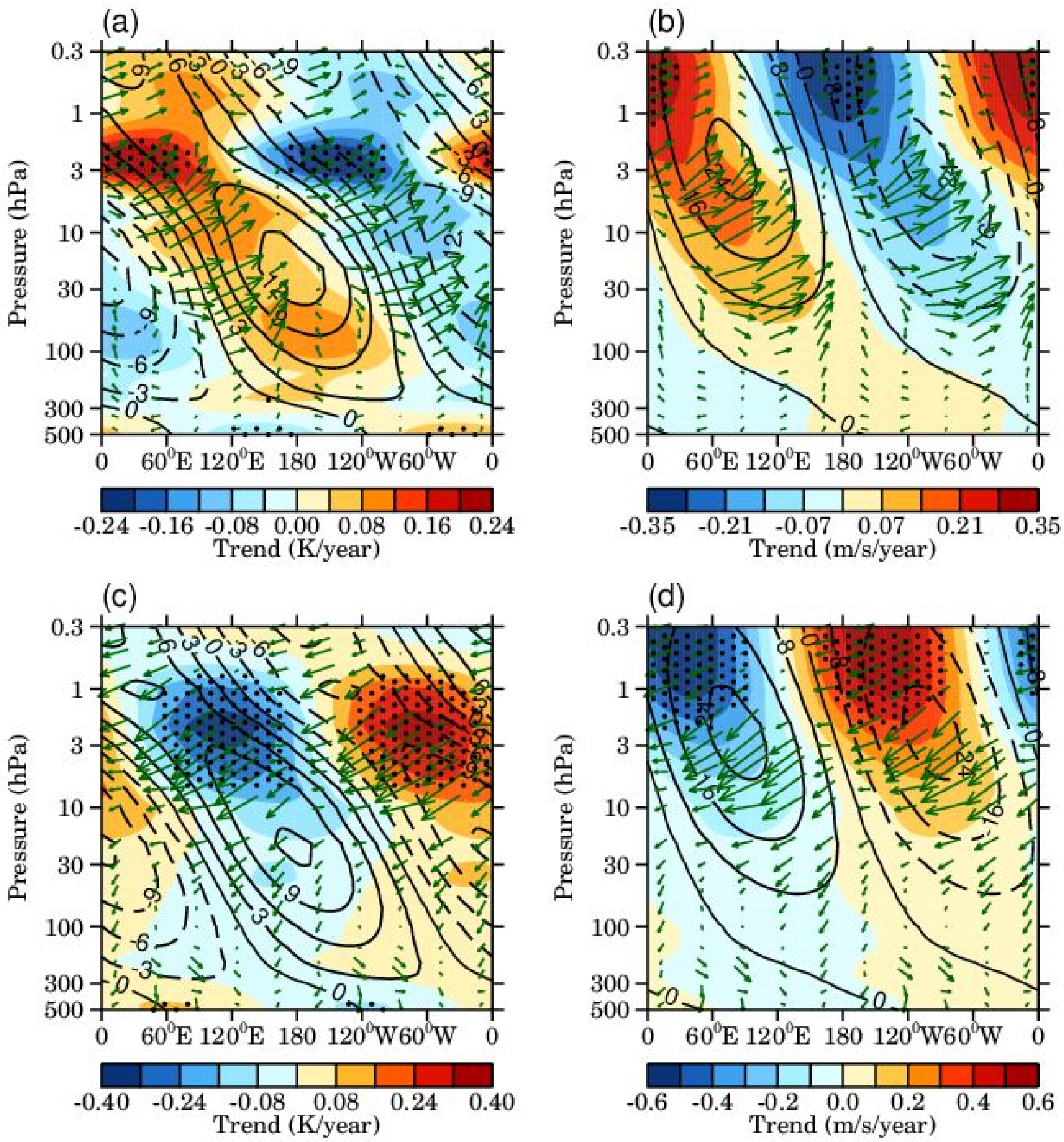

Fig. 5. Longitude-height cross sections of the trends (color shading) and climatology (black contours, the contour interval is 3 K, solid and dashed lines indicate positive and negative values, respectively) of (a) the temperature associated with wave 1 and (b) the meridional wind associated with wave 1 at 70°N from 1980 to 2003, respectively. (c) and (d) are the same as (a) and (b), respectively, but the time period is from 2003 to 2020. The green vectors denote Plumb flux trends associated with wave 1 (units in the horizontal and vertical components are 10^{-2} and 10^{-4} m^2/s^2/year, respectively). The vertical and horizontal wave fluxes are multiplied by the square root of 1000/pressure

(hPa). The stippled areas are statistically significant at the 95% confidence level according to Student's t test. The results are derived from the MERRA-2 dataset.

The long-term correlations between the zonally asymmetric temperature variations and the corresponding wave 1 component are shown in Fig. 6. The black line denotes the time series of the temperature differences between the climatology high-temperature region (50°N-70°N, 30°E-180°E) and climatology low-temperature region (50°N-70°N, 0-150°W) at 3 hPa (hereafter referred to as East–West) during January from 1980 to 2020 derived from the MERRA-2 reanalysis dataset. The red line denotes the time series of the vertical wave flux associated with wave 1 averaged between 40°N-70°N at 3 hPa (hereafter referred to as Fz1) during January from 1980 to 2020 derived from the MERRA-2 reanalysis dataset. It is seen that there is a strong correlation between wave 1 and hemispheric temperature differences near the stratopause. The correlation coefficient between Fz1 and East–West is 0.79 (0.77 when removing their linear trends), which is statistically significant at the 99% confidence level. Moreover, there is an apparent transition in the East–West (Fz1) around the 2000s, with a statistically significant increasing (decreasing) trend from 1980 to 2003 (2003 to 2020) during January. The increasing trend in East–West (Fz1) is 0.24 K/year (2.1×10^{-5} m^2/s^2/year), and the decreasing trend in East–West (Fz1) is -0.30 K/year (-2.7×10^{-5} m^2/s^2/year). Furthermore, Fz1 can explain 61% (64%) of the East–West variance and has a 60% (62%) contribution to the East–West trend from 1980 to 2003 (from 2003 to 2020) during January, as estimated from the linear regression method. Overall, the changes in the intensity of wave 1 can adequately explain the zonally asymmetric

temperature trends near the stratopause.

The East–West time series during January from 2003 to 2020 derived from TIMED/SABER observations is shown by the green line in Fig. 6. The East–West time series derived from TIMED/SABER observations agrees well with that derived from the MERRA-2 reanalysis dataset, with a 0.96 correlation coefficient.

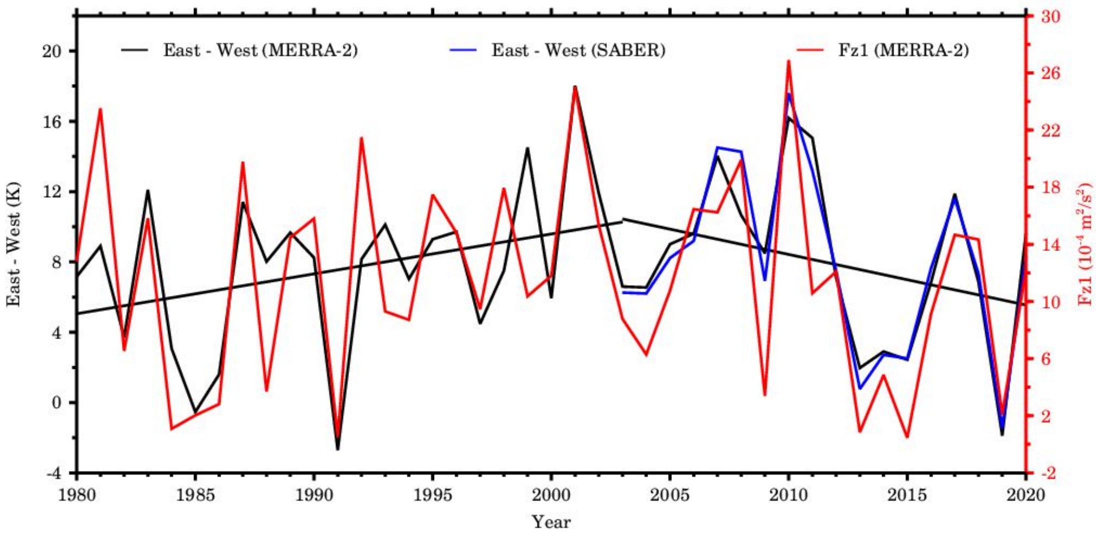

Fig. 6. Time series of the differences between the climatology of the high-temperature region (50°N-70°N, 30°E-180°E) and the climatology of the low-temperature region (50°N-70°N, 0-150°W) at 3 hPa (East–West) during January derived from the MERRA-2 reanalysis data (black line) and TIMED/SABER observations (green line), respectively, as well as the vertical wave flux associated with wave 1 (Fz1) averaged between 50°N - 70°N at 3 hPa (red line). The black straight lines are linear fits of the East–West during 1980–2003 and 2003–2020 derived from MERRA-2 reanalysis dataset.

It should be noted that the downwelling of the Brewer-Dobson circulation (BDC) may also affect the stratospheric temperature via adiabatic processes. Lin et al. (2009)

noted that enhanced BDC led to dynamic warming and produced a zonally ~~symmetric~~asymmetric structure along with ozone-induced radiative cooling in the lower and middle stratosphere during September and October from 1979 to 2007. Thus, a zonally ~~symmetric~~asymmetric pattern in temperature near the stratopause may be induced not only by the meridional advection of wave 1 but also by the effects of BDC. However, our analysis reveals that the residual vertical velocity in the stratosphere (i.e., the downwelling of BDC) does not have statistically significant changes, which agrees with Fu et al. (2019, Fig. 3). Therefore, the BDC contributes slightly to the zonally ~~symmetric~~asymmetric temperature trends during the study period.

The intensity of the stratospheric stationary planetary waves is affected by the tropospheric wave source (e.g., Matsuno, 1970). Thus, the shift in the intensity of wave 1 near the stratopause may also induced by the shift in intensity of tropospheric wave 1 source. Figs. 7a and 7b present the spatial map of trends in 500-hPa geopotential height associated with wave 1 during January from 1980-2003 and from 2003-2020 derived from MERRA-2 reanalysis dataset, respectively. Black contour lines overlapped in Figs. 7a and 7b denote the climatology of 500-hPa geopotential height associated with wave 1. It is seen that a transition in the intensity of the tropospheric wave 1 around the 2000s. There is a statistically significant increasing (decreasing) trend in the geopotential height over the eastern European and a statistically significant decreasing (increasing) trend in the geopotential height over North Pacific at mid-high latitude before (after) the 2000s, which is generally in phase (out of phase-) with the climatological eastern European high and the North Pacific low, respectively, indicating an enhanced

(weakened) wave 1 in the mid-high latitude troposphere before (after) the 2000s. Garfinkel et al. (2010) noted that the in phase (out of phase) of geopotential height anomalies in the eastern European high and the North Pacific low in the troposphere can constructively (destructively) interfere with the tropospheric wave 1 and thus enhance (weaken) the stratospheric wave 1.

Figs. 7c and 7d show the time series of the amplitude and phase anomaly of 500-hPa geopotential height associated with wave 1 at 70°N, respectively. The trend in wave 1 amplitude also underwent a transition before (1.6 m/year) and after (-1.1 m/year) the 2000s, which agrees with the results in Figs 7a and 7b. According to Smith et al. (2010), The increasing trend in phase of wave 1 before the 2000s (3.9 degree/year) and decreasing trend in phase of wave 1 after the 2000s (-3.3 degree/year), further supporting the constructively and destructively interfere with the tropospheric wave 1 before and after the 2000s, respectively.

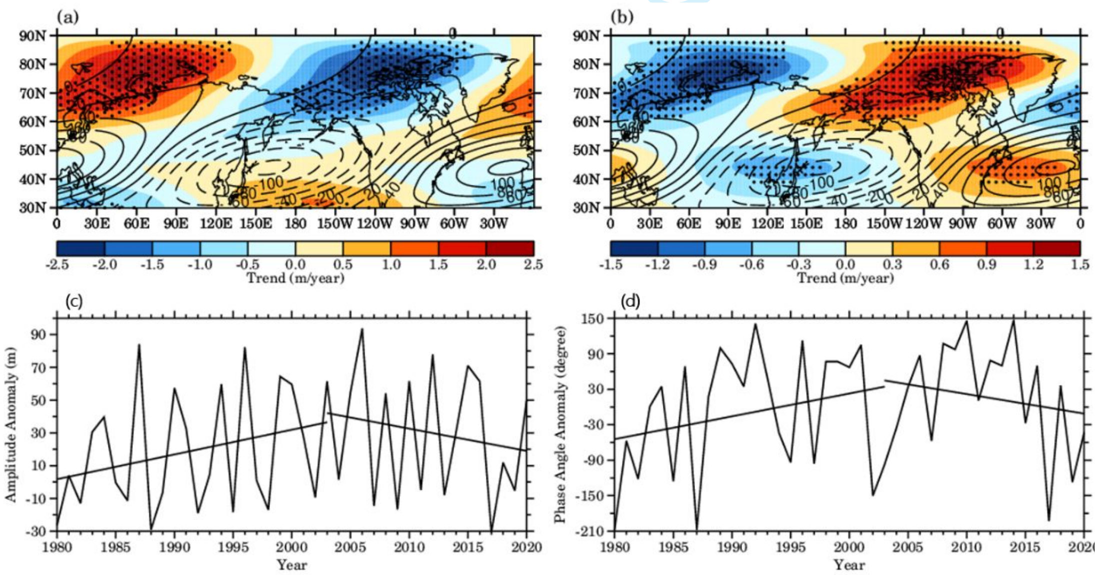

Fig. 7. (a) The spatial map of trends (color shading) and climatology (black contours, the contour interval is 20 m, solid and dashed lines indicate positive and negative values,

respectively) of 500-hPa geopotential height associated with wave 1 during January from 1980 to 2003 derived from MERRA-2 reanalysis data. (b) The same as (a), but the time period is from 2003 to 2020. The values over stippled areas are statistically significant at the 90% confidence level according to Student's t test. (c) Time series of the amplitude of 500-hPa geopotential height associated with wave 1 at 70°N. The black straight lines are linear fits of the amplitude during 1980–2003 and 2003–2020, respectively. (d) is the same as (c), but for the phase of 500-hPa geopotential height associated with wave 1.

5. Conclusion and Discussion

In this study, TIMED/SABER satellite observations and the MERRA-2 reanalysis dataset were used to investigate the spatial variations in the temperature trend near the NH stratopause during January from 1980 to 2020 and the possible factors responsible for these trends. We find that there is a zonally asymmetric temperature trend pattern near the northern mid-high latitude stratopause during January. There was a warming (cooling) trend in the eastern (western) hemisphere near the stratopause before the 2000s. However, a reversed zonally asymmetric temperature trend in the east-west direction was identified after the 2000s. Although the warming trends are statistically insignificant, they contrasted with the overall cooling trend in the upper stratosphere due to ozone depletion and increasing well-mixed GHGs in recent decades. Both datasets reveal that the zonal mean temperature has an overall cooling trend during the ~~NH~~northern winter near the stratopause. The temperature deviations from the zonal mean have similar zonally asymmetric trends and are in phase (out of phase) with the

climatology of the zonal temperature deviations before (after) the 2000s. Moreover, the zonally asymmetric trend in zonal temperature deviations tilts westward with height in the USLM and is most pronounced near the stratopause. The results derived from the MERRA-2 reanalysis dataset agree well with those derived from TIMED/SABER temperature observations in both morphology and magnitude during the TIMED/SABER satellite era.

Further analysis reveals that the meridional perturbation of wave 1 dominates the meridional wind near the stratopause, resulting in the zonally asymmetric pattern of the zonal temperature deviations. The increasing (decreasing) trend in the strength of wave 1 enhances (reduce) its meridional temperature advection near the stratopause before (after) the 2000s. Consequently, zonally asymmetric temperature trends alter in the east-west direction after (before) the 2000s. The effects of meridional temperature advection of wave 1 on the temperature in the USLM have also been reported in previous studies (e.g., Gabriel et al., 2011a). The results derived from the MERRA-2 reanalysis dataset indicate that wave 1 has a close correlation with the zonally asymmetric temperature pattern, with a statistically significant correlation coefficient of 0.79 (0.77 when removing their linear trends). The temperature variations associated with wave 1 can explain 61% (64%) of the variance in the zonally asymmetric temperature variations and contribute 60% (62%) to the zonally asymmetric temperature trend during January from 1980 to 2003 (from 2003 to 2020).

The tropospheric wave 1 at mid-high latitudes shows a strengthening (weakening) trend during January from 1980 to 2003 (from 2003 to 2020), which is in accordance

with the transition in the trend of stratospheric wave 1 intensity around the 2000s. The in phase (out of phase) of 500-hPa geopotential height anomalies in the eastern European high and the North Pacific low can constructively (destructively) interfere with the tropospheric wave 1 and thus enhance (weaken) the stratospheric wave 1 before (after) the 2000s. In addition, some studies have reported that the zonally asymmetric temperature variations near the stratopause can be modulated by 11-year solar cycles via their impact on wave 1 (Kodera and Kudora, 2002; Gabriel et al., 2011b; Liu et al., 2023). The effects of 11-year solar cycles on the zonally asymmetric temperature pattern will be investigated in future work.

Acknowledgments. We thank Han-Li Liu, William Randel, Fei Xie, Dingzhu Hu, Jiankai Zhang and Jinlong Huang for their helpful discussions and remarks. We would like to acknowledge the scientific teams at MERRA-2 and TIMED/SABER for providing the datasets.

Reference

Andrews, D. G., C. B. Leovy, and J. R. Holton, 1987: Middle atmosphere dynamics. Academic press.

Arblaster, J. M., N. P. Gillett, N. Calvo, et al., 2014: Stratospheric ozone changes and climate. *In Scientific assessment of ozone depletion: 2014.* World Meteorological Organization.

Chen, X. Y. and K. K., Tung, 2014: Varying planetary heat sink led to global-warming slowdown and acceleration. *Science*, **345**(6199), 897–903. https://doi.org/10.1126/science.1254937

Chipperfield, M. P., S. Bekki, S. Dhomse, et al., 2017: Detecting recovery of the stratospheric ozone layer. *Nature*, **549**(7671), 211-218, https://doi.org/10.1038/nature23681

Fu, Q., S. Solomon, and P. Lin, 2010: On the seasonal dependence of tropical lower-stratospheric temperature trends. *Atmospheric Chemistry & Physics*, **10**(6), 2643–2653, https://doi-org.cuucar.idm.oclc.org/10.5194/acp-10-2643-2010

Fu, Q., S. Solomon, H. A. Pahlavan, et al., 2019: Observed changes in Brewer–Dobson circulation for 1980–2018. *Environmental Research Letters*, **14**(11), 114026, doi: 10.1088/1748-9326/ab4de7

France, J. A., V. L. Harvey, C. E. Randall, et al., 2012: A climatology of stratopause temperature and height in the polar vortex and anticyclones. *Journal of Geophysical Research: Atmospheres*, **117**(D6), https://doi.org/10.1029/2011JD016893

France, J. A., and V. L. Harvey, 2013: A climatology of the stratopause in WACCM and the zonally asymmetric elevated stratopause. *Journal of Geophysical Research: Atmospheres*, **118**(5), 2241-2254, https://doi.org/10.1002/jgrd.50218

Funatsu, B. M., C. Claud, P. Keckhut, et al., 2016: Regional and seasonal stratospheric temperature trends in the last decade (2002–2014) from AMSU observations. *Journal of Geophysical Research: Atmospheres*, **121**(14), 8172-8185, https://doi.org/10.1002/2015JD024305

Golitsyn, G. S., A. I. Semenov, N. N. Shefov, et al., 1996: Long-term temperature trends in the middle and upper atmosphere, *Geophysical Research Letters*, **23**, 1741–1744, https://doi.org/10.1029/96GL01592

Gabriel, A., D. Peters, I. Kirchner, et al., 2007: Effect of zonally asymmetric ozone on stratospheric temperature and planetary wave propagation. *Geophysical Research Letters*, **34**(6), L06807, https://doi.org/10.1029/2006GL028998

Gabriel, A., H. Körnich, S. Lossow, 2011a: Zonal asymmetries in middle atmospheric ozone and water vapour derived from Odin satellite data 2001-2010. *Atmospheric Chemistry and Physics*, **11**(18), 9865-9885, https://doi-org.cuucar.idm.oclc.org/10.5194/acp-11-9865-2011

Gabriel, A., H. Schmidt, and D. H. W. Peters, 2011b: Effects of the 11-year solar cycle on middle atmospheric stationary wave patterns in temperature, ozone, and water vapor. *Journal of Geophysical Research: Atmospheres*, **116**(D23), https://doi.org/10.1029/2011JD015825

Garfinkel, C. I., D. L. Hartmann, and F. Sassi, 2010: Tropospheric precursors of anomalous Northern Hemisphere stratospheric polar vortices. *Journal of Climate*, **23**(12), 3282-3299. https://doi.org/10.1175/2010JCLI3010.1

Garcia, R. R., J. Yue, and J. M. Russell III, 2019: Middle atmosphere temperature trends in the twentieth and twenty‐first centuries simulated with the Whole Atmosphere Community Climate Model (WACCM). *Journal of Geophysical Research: Space Physics*, **124**(10), 7984-7993, https://doi.org/10.1029/2019JA026909

Gelaro, R., W. McCarty, M. J. Suárez, et al., 2017: The modern-era retrospective analysis for research and applications, version 2 (MERRA-2). *Journal of climate*, **30**(14), 5419-5454, https://doi.org/10.1175/JCLI-D-16-0758.1

Harvey, V. L., and M. H. Hitchman, 1996: A climatology of the Aleutian High. *Journal*

of the atmospheric sciences, **53**(14), 2088-2102, https://doi.org/10.1175/1520-0469(1996)053<2088:ACOTAH>2.0.CO;2

Harvey, V. L., R. B. Pierce, T. D. Fairlie, et al., 2002: A climatology of stratospheric polar vortices and anticyclones. *Journal of Geophysical Research: Atmospheres*, **107**(D20), ACL-10, https://doi.org/10.1029/2001JD001471

Hu, Y., and K. K. Tung, 2002: Interannual and decadal variations of planetary wave activity, stratospheric cooling, and Northern Hemisphere annular mode. *Journal of Climate*, **15**(13), 1659-1673, https://doi.org/10.1175/1520-0442(2002)015<1659:IADVOP>2.0.CO;2

Haynes, P., 2005: Stratospheric dynamics. *Annu. Rev. Fluid Mech.*, **37**, 263-293, doi: 10.1146/annurev.fluid.37.061903.175710

Hu, Y., and Q. Fu, 2009: Stratospheric warming in Southern Hemisphere high latitudes since 1979. *Atmospheric Chemistry and Physics*, **9**(13), 4329-4340. https://doi.org/10.5194/acp-9-4329-2009

Hu, Y., Y. Xia, M. Gao, and D. Lu, 2009: Stratospheric Temperature Changes and Ozone Recovery in the 21st Century, *J. Meteor. Res.*, **23**(3), 263-275.

Hu, D., W. Tian, F. Xie et al., 2015: Impacts of stratospheric ozone depletion and recovery on wave propagation in the boreal winter stratosphere. *Journal of Geophysical Research: Atmospheres*, **120**(16), 8299-8317, https://doi.org/10.1002/2014JD022855

Hu, D., Y. Guo, and Z. Guan, 2019: Recent weakening in the stratospheric planetary wave intensity in early winter. *Geophysical Research Letters*, **46**, 3953–3962,

https://doi.org/10.1029/2019GL082113

He, Y., X. Zhu, Z. Sheng, et al., 2022: Observations of Inertia Gravity Waves in the Western Pacific and Their Characteristic in the 2015/2016 Quasi - biennial Oscillation Disruption. *Journal of Geophysical Research: Atmospheres*, **127**, e2022JD037208, https://doi.org/10.1029/2021JD034719

Ivy, D. J., S. Solomon, and H. E. Rieder, 2016: Radiative and dynamical influences on polar stratospheric temperature trends. *Journal of Climate*, **29**(13), 4927-4938. DOI: https://doi.org/10.1175/JCLI-D-15-0503.1

Kodera, K., and Y. Kuroda, 2002: Dynamical response to the solar cycle. *Journal of Geophysical Research: Atmospheres*, **107**(D24), ACL-5, https://doi.org/10.1029/2002JD002224

Keckhut, P., C. Claud, B. Funatsu, et al., 2019: Temperature trends observed in the middle atmosphere and future directions. *Infrasound Monitoring for Atmospheric Studies: Challenges in Middle Atmosphere Dynamics and Societal Benefits*, 805-823, https://doi.org/10.1007/978-3-319-75140-5_26

Lin, P., Q. Fu, S. Solomon, et al., 2009: Temperature trend patterns in Southern Hemisphere high latitudes: Novel indicators of stratospheric change. *Journal of Climate*, **22**(23), 6325-6341, https://doi.org/10.1175/2009JCLI2971.1

Long, C. S., M. Fujiwara, S. Davis, et al., 2017: Climatology and interannual variability of dynamic variables in multiple reanalysis evaluated by the SPARC Reanalysis Intercomparison Project (S-RIP), *Atmos. Chem. Phys.*, **17**, 14593–14629, https://doi.org/10.5194/acp-17-14593-2017

Liu, H. L., M. Rempel, G. Danabasuglu, et al., 2023, Climate responses under an extreme quiet sun scenario. *Journal of Geophysical Research: Atmospheres,* e2022JD037626. https://doi.org/10.1029/2022JD037626

Matsuno, T., 1970: Vertical propagation of stationary planetary waves in the winter Northern Hemisphere. *Journal of Atmospheric Sciences*, **27**(6), 871-883. https://doi.org/10.1175/1520-0469(1970)027<0871:VPOSPW>2.0.CO;2

Matsuno, T., 1971: A dynamical model of the stratospheric sudden warming. *Journal of Atmospheric Sciences*, **28**(8), 1479-1494. https://doi.org/10.1175/1520-0469(1971)028<1479:ADMOTS>2.0.CO;2

Maycock, A. C., M. M. Joshi, K. P. Shine, et al., 2014: The potential impact of changes in lower stratospheric water vapour on stratospheric temperatures over the past 30 years. *Quarterly Journal of the Royal Meteorological Society*, **140**(684), 2176–2185, https://doi.org/10.1002/qj.2287

Maycock, A. C., W. J. Randel, A. K. Steiner, et al., 2018: Revisiting the mystery of recent stratospheric temperature trends. *Geophysical Research Letters*, **45**(18), 9919-9933, https://doi.org/10.1029/2018GL078035

McLandress, C., T. G. Shepherd, A. I. Jonsson, et al., 2015: A method for merging nadir-sounding climate records, with an application to the global-mean stratospheric temperature data sets from SSU and AMSU. *Atmospheric Chemistry and Physics*, **15**, 9271-9284, https://doi.org/10.5194/acp-15-9271-2015

Plumb, R. A., 1985: On the three-dimensional propagation of stationary waves. *Journal of the Atmospheric Sciences*, **42**(3), 217-229, https://doi.org/10.1175/1520-

0469(1985)042<0217:OTTDPO>2.0.CO;2

Ramaswamy, V., M. L. Chanin, J. Angell, et al., 2001: Stratospheric temperature trends: Observations and model simulations. *Reviews of Geophysics*, **39**(1), 71-122, https://doi.org/10.1029/1999RG000065

Randel, W. J., K. P. Shine, J. Austin, et al., 2009: An update of observed stratospheric temperature trends. *Journal of Geophysical Research: Atmospheres*, **114**(D2), https://doi.org/10.1029/2008JD010421

Randel, W. J., A. K. Smith, F. Wu, et al., 2016: Stratospheric temperature trends over 1979–2015 derived from combined SSU, MLS, and SABER satellite observations. *Journal of Climate*, **29**(13), 4843-4859, https://doi.org/10.1175/JCLI-D-15-0629.1

Remsberg, E., G. Lingenfelser, V. L. Harvey, et al., 2003: On the verification of the quality of SABER temperature, geopotential height, and wind fields by comparison with Met Office assimilated analyses. *Journal of Geophysical Research: Atmospheres*, **108**(D20), 4628, https://doi.org/10.1029/2003JD003720

Remsberg, E. E., B. T. Marshall, M. Garcia-Comas, et al., 2008: Assessment of the quality of the Version 1.07 temperature-versus-pressure profiles of the middle atmosphere from TIMED/SABER. *Journal of Geophysical Research: Atmospheres*, **113**, D17101, https://doi.org/10.1029/2008JD010013

Remsberg, E., 2019: Observation and attribution of temperature trends near the stratopause from HALOE. *Journal of Geophysical Research: Atmospheres* 124.12, 6600-6611, doi: 10.1029/2019JD030455

Shine, K. P., M. S. Bourqui, P. D. F. Forster, et al., 2003: A comparison of

model-simulated trends in stratospheric temperatures. *Quarterly Journal of the Royal Meteorological Society*, **129**(590), 1565-1588, https://doi.org/10.1256/qj.02.186

Smith, K. L., C. G. Fletcher, and P. J. Kushner, 2010: The role of linear interference in the annular mode response to extratropical surface forcing. *Journal of Climate*, **23**(22), 6036-6050. https://doi.org/10.1175/2010JCLI3606.1

Seidel, D. J., N. P. Gillett, J. R. Lanzante, et al., 2011: Stratospheric temperature trends: Our evolving understanding. *Wiley Interdisciplinary Reviews: Climate Change*, **2**(4), 592-616, https://doi.org/10.1002/wcc.125

Seidel, D. J., J. Li, C. Mears, et al., 2016: Stratospheric temperature changes during the satellite era. *Journal of Geophysical Research: Atmospheres*, **121**(2), 664-681, https://doi.org/10.1002/2015JD024039

Rao, J., R. Ren, and Y. Yang, 2015: Parallel comparison of the northern winter stratospheric circulation in reanalysis and in CMIP5 models. *Advances in Atmospheric Sciences*, **32**, 952-966. https://doi.org/10.1007/s00376-014-4192-2

Steiner, A. K., F. Ladstädter, W. J. Randel, et al., 2020: Observed temperature changes in the troposphere and stratosphere from 1979 to 2018. *Journal of Climate*, **33**(19), 8165-8194. DOI: https://doi.org/10.1175/JCLI-D-19-0998.1

Thompson, D. W., and S. Solomon, 2009: Understanding recent stratospheric climate change. *Journal of Climate*, **22**(8), 1934-1943, https://doi.org/10.1175/2008JCLI2482.1

Thompson, D. W., D. J. Seidel, W. J. Randel, et al., 2012: The mystery of recent stratospheric temperature trends. *Nature*, **491**(7426), 692-697,

https://doi.org/10.1038/nature11579

Wang, L., C.-Z. Zou, and H. Qian, 2012: Construction of stratospheric temperature data records from stratospheric sounding units. *J. Climate*, **25**, 2931–2946, doi:10.1175/JCLI-D-11-00350.1.

WMO, 2018: *WMO statement on the state of the global climate in 2017*. World Meteorological Organisation, Geneva.

Xia, Y., Xu, W., Hu, Y. et al., 2020: Southern-Hemisphere high-latitude stratospheric warming revisit. Clim Dyn 54, 1671–1682. https://doi.org/10.1007/s00382-019-05083-7

Yamashita, C., H. L. Liu, and X. Chu, 2010: Gravity wave variations during the 2009 stratospheric sudden warming as revealed by ECMWF‐T799 and observations. *Geophysical Research Letters*, **37**(22), https://doi.org/10.1029/2010GL045437

Zou, C. Z., M. Gao, and M. D. Goldberg, 2009: Error structure and atmospheric temperature trends in observations from the Microwave Sounding Unit. *Journal of Climate*, **22**(7), 1661-1681, https://doi.org/10.1175/2008JCLI2233.1

Zou, C. Z., and H. Qian, 2016: Stratospheric temperature climate data record from merged SSU and AMSU-A observations. *Journal of Atmospheric and Oceanic Technology*, **33**(9), 1967-1984, https://doi.org/10.1175/JTECH-D-16-0018.1

Zhou, L., Y. Xia, and C. Zhao, 2022: Influence of Stratospheric Ozone Changes on Stratospheric Temperature Trends in Recent Decades, *Remote Sensing*, **14**(21), 5364. https://doi.org/10.3390/rs14215364